JOURNAL OF GEOPHYSICAL RESEARCH, VOL. 114, C11015, doi:10.1029/2008JC005158, 2009

Click Here for Full Article

Surf zone diffusivity on a rip-channeled beach

Jeff Brown,[1] Jamie MacMahan,[2] Ad Reniers,[3,4] and Ed Thornton[2]

Received 16 October 2008; revised 16 June 2009; accepted 21 July 2009; published 14 November 2009.

[1] Absolute and relative diffusivity are measured on a rip-channeled beach using 30 position-tracking drifters released in clusters (4–12 drifters) deployed on 7 days with different wave forcing and tidal elevations at Sand City, Monterey Bay, California. Diffusivity and dispersion were found to be larger on days with rip current flow patterns and larger waves. Rip currents cause material to diffuse quickly for $t < 90$ s in the cross shore (κ_{xx} = 5.4–6.1 m^2/s) before decreasing to an asymptotic oscillation (κ_{xx} = 0.9–2.2 m^2/s), while alongshore material diffusion is initially ($t < 170$ s) smaller than cross-shore diffusion and asymptotes at a larger value (κ_{yy} = 2.8–3.8 m^2/s). The cross- and alongshore absolute diffusivity modulate at ~300 s corresponding to the average circulation time for a rip current. Two-particle relative dispersion (D_p) grows like $D_p^2 \sim t^{4/3}$ and the relative diffusivity (K_p) is scale dependent, $K_p \sim d^{0.2}$ (d is particle separation). Cluster relative diffusion (K_e) ranged from 1.0 to 4.5 m^2/s and cluster relative dispersions (D_e) are significantly correlated with two-particle relative dispersions (D_S) [$R^2 > 0.9$]. Two independent methods are used to measure the small-scale turbulent diffusion contribution (k_{xy}), which are found significantly correlated ($R^2 = 0.95$) with each other and calculated surf zone wave breaking induced turbulent eddy viscosity. Here k_{xy} is small relative to the total dispersion (K_e/k_{xy} = 3–30), indicating that the shear flow is the primary mechanism responsible for dispersion in a rip current system.

Citation: Brown, J., J. MacMahan, A. Reniers, and E. Thornton (2009), Surf zone diffusivity on a rip-channeled beach, *J. Geophys. Res.*, *114*, C11015, doi:10.1029/2008JC005158.

1. Introduction

[2] The importance of rip currents in dispersing material across the surf zone and nearshore is highlighted by *Inman et al.* [1971], *Johnson and Pattiaratchi* [2004], *Grant et al.* [2005], and *Clarke et al.* [2007]. A rip current is a seaward-flowing jet of water that originates near the shoreline, extends across the surf zone, and episodically exits the surf zone [*Shepard et al.*, 1941; *MacMahan et al.*, 2006, 2009a]. The mean Lagrangian flow in a rip current was measured using Global Positioning System (GPS) equipped drifters during the Rip Current Experiment (RCEX) at Sand City, Monterey Bay, California, documenting large velocities and shear within the surf zone [*MacMahan et al.*, 2009a]. The effect of rip currents on dispersing material is not well understood.

[3] A patch of fluid (tracer) advected in a turbulent flow is distorted and translated by the flow after its release. The dispersal effects of the turbulent velocities on the patch can be parameterized by the two types of "eddy" diffusivity, absolute and relative [*Richardson*, 1926; *Davis*, 1987; *LaCasce and Bower*, 2000; *Spydell et al.*, 2007]. Absolute diffusivity (κ) corresponds to the ensemble averaged behavior of a patch of marked fluid over many independent releases in a coordinate frame originating at an "inferred" common release point and is calculated as the rate of change of the variance of the particle displacements from their starting positions (absolute dispersion, σ^2). It characterizes the translation effects of the mean current on the particles. Relative diffusivity (K) and relative dispersion (D^2) relate to the distortion of the tracer and refer to the spreading of the cloud in a reference frame fixed to the cloud's center of mass [*Richardson*, 1926]. When particle behavior becomes decorrelated, the relative diffusivity and absolute diffusivity are approximately equal [*LaCasce and Bower*, 2000]. One-particle statistics are used to estimate absolute diffusivity (κ), whereas relative diffusivity is estimated with two particle (K_p) or cluster (K_e) statistics. A summary of diffusivity notation previously used within the nearshore is provided in Table 1. *Richardson* [1926] found in atmospheric turbulence observations that relative diffusivity is dependent on spatial separations (l), $K \sim l^{4/3}$, and that relative dispersion is dependent on time, $D^2 \sim t^3$. Richardson-like relationships have been observed in geophysical flows [*Okubo*, 1971; *LaCasce and Bower*, 2000] and the time scaling has been supported both theoretically [*Obukhov*, 1941a, 1941b; *Batchelor*, 1950], in 2-D and 3-D turbulence models [*Boffetta and Sokolov*, 2002a,

[1]Civil and Environmental Engineering, University of Delaware, Newark, Delaware, USA.
[2]Oceanography Department, Naval Postgraduate School, Monterey, California, USA.
[3]Department of Hydraulic Engineering, Delft University of Technology, Delft, Netherlands.
[4]Applied Marine Physics, Rosenstiel School of Marine and Atmospheric Science, University of Miami, Miami, Florida, USA.

Copyright 2009 by the American Geophysical Union.
0148-0227/09/2008JC005158$09.00

Table 1. Description of Diffusivity Notation Described Herein and for the Literature Cited Herein

Notation	Description	Cited Literature
κ (κ_{xx}, κ_{yy})	Absolute diffusivity computed from one-particle statistics	ε from *Inman et al.* [1971], D from *Clarke et al.* [2007], D_{eff} from *Grant et al.* [2005]
σ (σ_{xx}, σ_{yy})	Patch size (standard deviation) computed from single particle statistics	β from *Spydell et al.* [2007]
K_p (K_{pxx}, K_{pyy})	Relative diffusivity computed from two-particle statistics	μ from *Spydell et al.* [2007]
D_p (D_{px}, D_{py})	Relative dispersion computed from two-particle statistics	D_{xx} or D_{yy} from *Spydell et al.* [2007]
K_e (K_{ex}, K_{ey})	Relative diffusivity computed from two-particle statistics	K (called relative dispersion) from *Johnson and Pattiaratchi* [2004]
D_e (D_{ex}, D_{ey})	Relative dispersion computed from cluster statistics	σ from *Smith* [1989], *List et al.* [1990], *Drinkwater and Loder* [2001], and *Manning and Churchill* [2006]
k (k_x, k_y, k_{xy})	Turbulent eddy diffusivity calculated from cluster method	*Okubo and Ebbesmeyer* [1976] and *List et al.* [1990]

2002b] and in laboratory experiments of 2-D turbulence [*Jullien et al.*, 1999].

[4] Until recently, the studies measuring nearshore dispersion within the surf zone focused on dye dilution and the results produced varying estimates of diffusivity. *Inman et al.* [1971] found values of absolute cross-shore diffusivity (κ_{xx}) between 0.1 and 5.9 m^2/s and absolute alongshore diffusivity (κ_{yy}) between 0.0 and 0.17 m^2/s for different wave conditions on two beaches featuring rip currents. *Clarke et al.* [2007] fit a series of nearshore dye concentration measurements to diffusion models to calculate the variance of the particle displacement and obtained values of κ of $O(10^{-1}-10^{3})$ m^2/s depending on the wave conditions and the presence of rip currents; model estimates of κ_{xx} and κ_{yy} were generally larger, $O(10^{0}-10^{3}$ $m^2/s)$, in the presence of rip currents. *Grant et al.* [2005] measured dye spreading on mostly planar beaches cut with irregularly spaced (100–1000 m) rip channels over longer times ($O(10^3$ s)) and estimated $40 < \kappa_{yy} < 80$ m^2/s with larger values for larger waves.

[5] Position-tracking drifters are also used to estimate diffusivity (dispersion). Previously the position accuracy and temporal and spatial scales of motions of interest have limited the use of drifters to general ocean circulation or other large scale, O(10s of km), O(days), motions [*Davis*, 1985; *Smith*, 1989; *Sanderson*, 1995; *LaCasce and Bower*, 2000; *Drinkwater and Loder*, 2001; *Tseng*, 2002; *Manning and Churchill*, 2006]. The size of the drifters were O(1–10 m) with position fixes O(0.25–1 h), which is not adequate for use within the surf zone. The increasing accuracy and declining cost/size of GPS units made it possible to track small drifters within the surf zone [*Schmidt et al.*, 2003, 2005; *Johnson et al.*, 2003; *Johnson and Pattiaratchi*, 2004; *Spydell et al.*, 2007; *MacMahan et al.*, 2009b].

[6] *Spydell et al.* [2007] repeatedly deployed nine surf zone drifters on a sandy beach with minimal alongshore bathymetric variations on 2 separate days. They were able to resolve the alongshore current flow field over an area 250 m in the alongshore and 200 m in the cross shore. Applying the formulations of *Taylor* [1922] and *Davis* [1987], absolute (κ) and relative (K_p) diffusivities were estimated from the ensemble Lagrangian drifter data. Values of $\kappa_{xx} = 0.7$ m^2/s and $\kappa_{yy} = 2.0$ m^2/s were calculated on a day with predominantly shore normal waves and small significant wave height, $H_s = 0.5$ m, that resulted in weak alongshore currents ($|\overline{v}| < 0.1$ m/s). Larger values of $\kappa_{xx} = 1.5$ m^2/s and $\kappa_{yy} = 4.3$ m^2/s were obtained for a day with larger, $H_s = 1.4$ m and obliquely incident waves that induced a strong alongshore current ($|\overline{v}| = 0.5$ m/s). They found weaker than Richardson-like dependence with $D_p^2 \sim t^{3/2}$ and $K_p \sim l^{2/3}$.

[7] *Johnson and Pattiaratchi* [2004] deployed four position-tracking drifters in clusters in a transient rip current and found cluster-estimated total relative diffusivities, K_e, from 0.7 to 1.9 m^2/s that supported Richardson-like behavior. Note that the reported values of 1.3 and 3.9 m^2/s were found to be incorrect after further inspection of the figures provided by *Johnson and Pattiaratchi* [2004]. Alongshore (corrected) relative diffusivities (0.9–2.9 m^2/s) were found to be larger than (corrected) cross shore (−0.4 to 1.0 m^2/s).

[8] Thirty GPS-tracking surf zone drifters were repeatedly redeployed on a sandy beach with quasiperiodic alongshore spaced (O(125 m)) rip channels [*MacMahan et al.*, 2005, 2009a, 2009b], the results of which form the basis of this paper. Absolute (one-particle statistics) and relative (two-particle and cluster statistics) diffusivity and dispersion are evaluated under various wave forcing and tidal elevations for the different flow patterns observed on a rip channeled beach. Drifters were released in clusters so that estimates of cluster statistics and ensemble statistics could be compared. *LaCasce* [2008] suggested that the two methods should provide similar relationships, but no field comparison had been performed to date. Comparisons are made to other surf zone diffusivity studies focusing on the effects of rip current motions in dispersing material. The rotational effects associated with the rip current vortices and their influence on particle diffusion are explored [*Veneziani et al.*, 2004, 2005a, 2005b]. The small-scale turbulent diffusivity [*Okubo and Ebbesmeyer*, 1976; *List et al.*, 1990] is calculated using two independent methods to determine the relative importance of the shear compared with breaking wave-induced turbulence.

2. Observations

[9] Drifter deployments were performed on 7 different days in late April and early May 2007, at Sand City, Monterey Bay, California, as part of the RCEX. The experimental site was chosen for the year-round persistent rip channels (currents) owing to the predominantly nearshore normal incident waves [*MacMahan et al.*, 2005]. Drifters spanned roughly 400 m in the alongshore and 200 m in the cross shore and included a minimum of 3 rip channels spaced ~125 m in the alongshore. The experi-

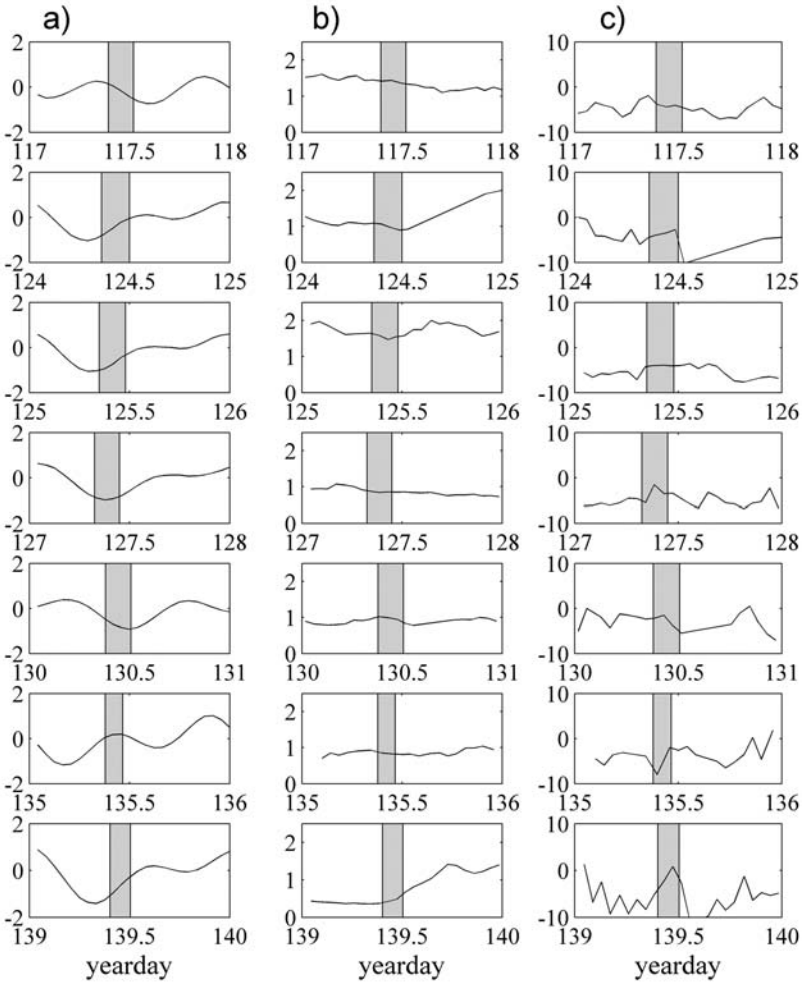

Figure 1. (a) Tidal elevation measured in meters at local NOAA station (9413450). (b) Significant wave height (H_s) in meters and (c) peak wave direction (degrees) relative to shore normal, with positive to the south for the drifter deployments measured in 13 m water depth. The shaded area outlines the time the drifters were in the ocean.

mental setup and deployment conditions are described in greater detail by *MacMahan et al.* [2009a]. All deployments occurred in the morning (Table 2) to avoid adverse windage effects from afternoon sea breeze events. Drifter deployments lasted between 2 and 3 h, depending on the conditions and available work force. The mean tidal elevations ranged from −0.8 to 0.3 m relative to mean sea level. Deployments were made at high, low, and rising and falling midtides (Figure 1 and Table 2). The peak wave directions measured in 13 m water depth were near normally incident ($\theta_p = -6.1$ to $-5.7°$) for all deployments. The significant wave heights for the first five deployments ($H_s = 0.9–1.6$ m) were larger than the wave heights of the last 2 days ($H_s = 0.5–0.8$ m). The peak period ($T_p = 6–14$ s) also decreased for the last 2 deployment days. Concomitant with decreasing wave height and period, the flow patterns changed from a rip current circulation to a sinuous alongshore current coupled to the rip channel morphology.

[10] The drifters are modified from the design of *Schmidt et al.* [2003] and consist of a central tube of 0.1 m diameter PVC, flat circular pieces of PVC and steel affixed to the bottom to act as dampener and ballast, and a 0.7 m long antenna mast of 0.03 m diameter PVC rising from the top. The drifters are weighted so that only the central tube is in the water [see *MacMahan et al.*, 2009b, Figure 5]. The drifters are tracked by internally recording (0.5 Hz) handheld Earthmate Blue Logger GPS units that after modification have a dynamic position and velocity error of 0.4 m and 0.01 m/s. Drifter velocities compared well with in situ Eulerian measurements (correlation coefficient $r = 0.7$) and drifters followed dye patches when simultaneously released [*MacMahan et al.*, 2009b].

[11] Drifters were released in clusters of 4–12 drifters near the shoreline in wading depths. Once released, the drifters were allowed to migrate freely until they either beached or exited the area of interest, where they were removed from the water. When more than four drifters were removed from the water, a new cluster was redeployed. The number of cluster deployments varied with the surf zone conditions and corresponding surf zone retention, from two clusters on yearday 125 (rip current flow pattern) to 7 on yearday 139 (alongshore current flow pattern).

Table 2. Drifter Deployments[a]

Yearday	Start (LT)	Duration	H_s (m)	T_p (s)	θ_p (deg)	X_s (m)	Mean Sea Level (m)	Flow Pattern	Surf Zone Exits (%)
117	0928	3 hours	1.4	11.4	−4.3	155	−0.1 high	Rip	7
124	0838	3 hours 24 min	1.0	13.9	−4.7	126	−0.3 rising	Rip	6
125	0822	3 hours 8 min	1.6	8.5	−4.5	140	−0.6 rising	Rip	2
127	0748	2 hours 59 min	0.9	8.8	−4.9	122	−0.8 low	Meandering	23
130	0908	3 hours 1 min	1.0	9.6	−4.5	120	−0.7 falling	Meandering	16
135	0907	2 hours 4 min	0.8	7.8	−4.5	90	0.3 high	Meandering	2
139	0938	2 hours 28 min	0.5	6.0	−6.1	105	−0.5 rising	Sinuous	6

[a]Here H_s is the significant wave height, T_p is the peak period, and θ_p is the peak wave direction; X_s(m) is the estimated surf zone width. Mean sea level is the tidal level relative to mean sea level and was measured at local NOAA station. Flow pattern is the current classification for each deployment and surf zone exits represents the percentage of drifters exiting the surf zone after entering a rip channel.

[12] The time series of drifter positions recorded by the GPS units were converted to a local coordinate system and were filtered to remove erroneous points. Gaps were filled with spline interpolation if less than 10 s and linear interpolation if longer than 10 s [*Spydell et al.*, 2007]. Velocity estimates were computed using a forward-differencing scheme.

[13] The following three different surf zone flow patterns were observed over the seven drifter deployments: (1) rip current, (2) meandering flow field, and (3) sinuous alongshore current [*MacMahan et al.*, 2009a]. The meandering flow pattern is a combination of the rip and alongshore current patterns, with the drifters moving back and forth across the surf zone along constant isobaths, frequently ignoring the rip channels, but at times circulating around a rip current cell a few times. The last flow field is the sinuous alongshore flow pattern which consists of an alongshore current that moves the drifters along a relatively constant isobath and bears little or no resemblance to the traditional view of rip currents or alongshore currents. Yeardays 117, 124, and 125 exhibit the rip current pattern; yeardays 127, 130, and 135 exhibit the meandering flow pattern; and yearday 139 exhibits the sinuous alongshore current pattern (Table 2).

3. Absolute Diffusivity: One-Particle Statistics

[14] The average tracer evolution from a common release point can be described with one-particle statistics. The relative position displacement of a drifter is computed for a relative time step t' by subtracting a specified position at an earlier time, $\boldsymbol{x}(t'_0)$, from the position at a time t' seconds later, $\boldsymbol{x}(t'_0 + t')$. The collection of relative position displacements represents the "particle" paths. A mean displacement of the particle paths is computed from the ensemble. The assumption of a spatially homogeneous and temporally stable (stationary) flow field allows the random motions represented by the particle trajectories to be described in the same manner as the bulk molecular diffusion [*Taylor*, 1922]. Under these assumptions, all "particles" can be viewed as originating from a common release point in space and time regardless of originating drifter positions $\boldsymbol{x}(t'_0)$. The probability density function (pdf) of the individual particle displacements about the mean particle displacement represents the ensemble-averaged anomalous displacements, describing the spread of a tracer and quantifying the translation of the particles resulting from the mean flow [*LaCasce and Bower*, 2000]. The rate of pdf spreading (measured as the change in time of the variance, σ^2) is quantified as absolute diffusivity, κ, with

$$\kappa_{ij} = \frac{1}{2}\frac{d}{dt'}\sigma^2_{ij}(t'), \tag{1}$$

where $i, j = x, y$ and σ^2_{ij} is the second moment of displacements

$$\sigma^2_{ij}(t') = \int\int r'_i r'_j P\left(r'_x, r'_y; t'\right) dr'_i dr'_j. \tag{2}$$

$P(r_x', r_y'; t')$ is the pdf of the anomalous particle displacements $\boldsymbol{r}'$ (r_x': cross-shore and r_y': alongshore displacement). The above assumption of a homogeneous and stationary flow field allows additional (not independent) data to be introduced into the pdf estimate. The relative position displacement of a single drifter after t' seconds, $\boldsymbol{r}(t') = \boldsymbol{x}(t'_0 + t') - \boldsymbol{x}(t'_0)$, is calculated for all t'_0 arbitrary starting positions. One drifter time series of N total position measurements yields $(N-1)$ values for $\mathbf{r}(t' = 2\text{ s})$, $(N-2)$ values for $\boldsymbol{r}(t' = 4\text{ s})$ etc, as particle displacements are calculated for all $t' = 0, 2, 4, 6\ldots$ s from $t'_0 = 0, 2, 4\ldots$ s with positions sampled at $\Delta t = 2$ s. Anomalous relative position displacements are calculated for each time step t' as $\boldsymbol{r}'(t') = \boldsymbol{r}(t') - \boldsymbol{R}(t')$, where $\boldsymbol{R}(t')$ is the mean spatial displacement for all drifters at all arbitrary t'_0 [*Batchelor and Townsend*, 1956; *Spydell et al.*, 2007]. The ensemble average evolution of the initial point source of a tracer is related to the rate of change of the pdf of the anomalous displacements, $P(r_x', r_y'; t')$.

[15] The distribution of $P(r_x', r_y'; t')$ appears close to circular under visual evaluation for $t' < 100$ s regardless of flow pattern (Figure 2), but calculations of the pdf variances (from (2)) reveal slight polarizations in the distributions. The pdfs are slightly polarized in the cross-shore direction, r_x', for all flow patterns for $t' < 30$ s. $P(r_x', r_y'; t')$ becomes circular and then slightly alongshore polarized as t' increases for all flow patterns (Table 3). This transition occurs faster on yearday 130 ($t' = 30$ s) than for other deployment days ($t' = 200$–400 s). This can be explained by the differences in drifter paths as some drifters moved alongshore while others remained trapped in a rip current cell, causing more variation in the alongshore displacements. The unidirectional alongshore current with smaller waves on yearday 139 results in the smallest spread and causes an asymmetrical distribution in the positive alongshore anomalous position displacements (Figures 2m–2p)

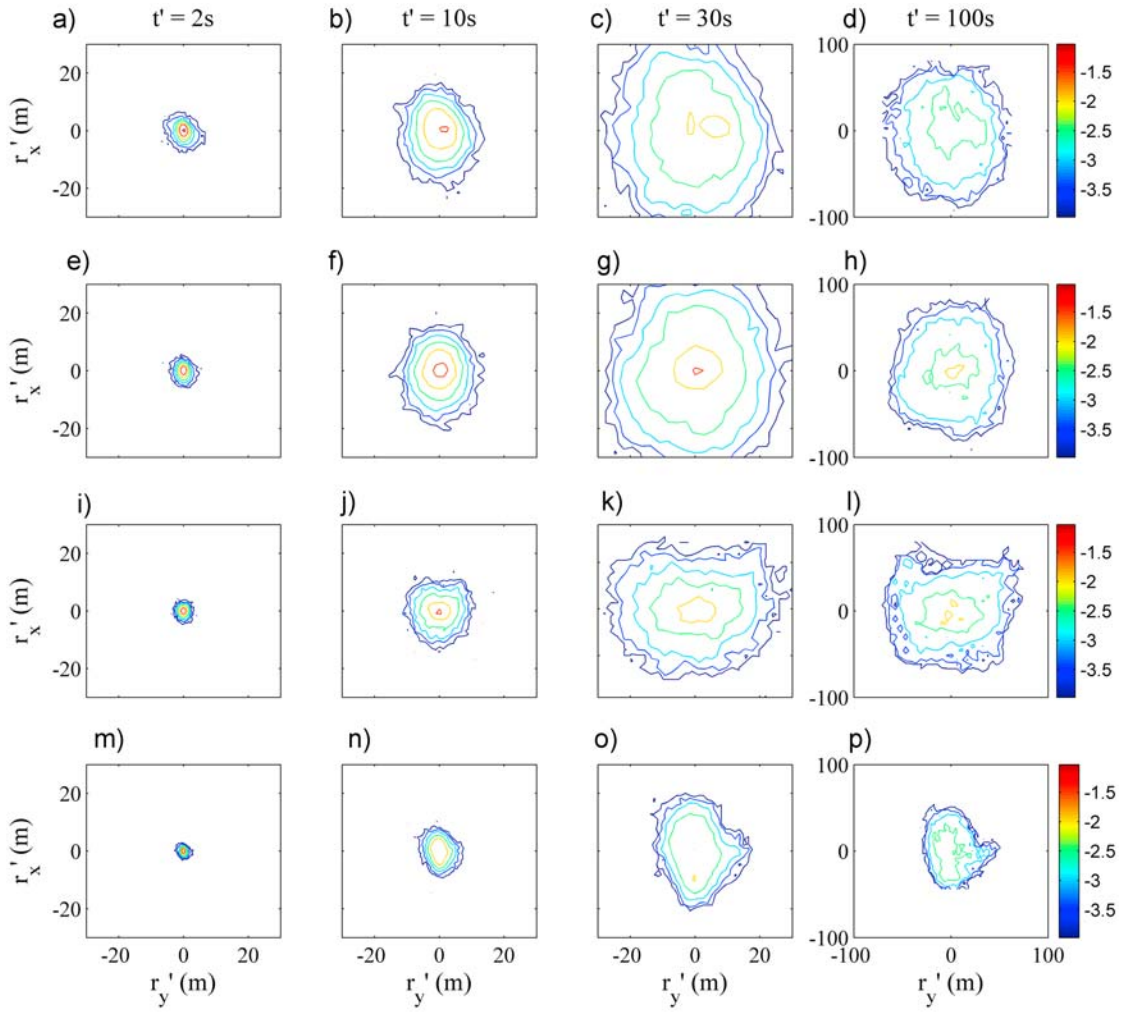

Figure 2. Plots of $\log_{10}[P(r'_x, r'_y; t')]$ for yeardays (a–d) 117, (e–h) 124, (i–l) 130, and (m–p) 139 at $t' = 2$ s (Figures 2a, 2e, 2i, and 2m), 10 s (Figures 2b, 2f, 2j, and 2n), 30 s (Figures 2c, 2g, 2k, and 2o), and 100 s (Figures 2d, 2h, 2l, and 2p). Contours are $\log_{10}[P(r_x', r_y'; t')] = -4, -3.5, \ldots -1.5, -1$. Note the change of axis for the $t' = 100$ s plots.

instead of the alongshore symmetric particle displacement distribution seen on yearday 130 when the mean alongshore current switched directions midway through the deployment (Figures 2i–2l).

[16] In a stationary and homogeneous flow field, the absolute dispersion or variance σ^2, defined as the particle deviation from the mean particle displacement, can also be computed directly from the particle displacements as

$$\sigma_{ij}^2(t') = \sum^{particles} \left(x_i(t') - \langle x_i(t')\rangle\right)\left(x_j(t') - \langle x_j(t')\rangle\right) \quad (3)$$

Table 3. Absolute Diffusivity[a]

Yearday	$t(\mathrm{mx}(\kappa_{xx}))$ (s)	$\mathrm{mx}(\kappa_{xx})$ (m^2/s)	κ_{xx}^{∞} (m^2/s)	$t(\mathrm{mx}(\kappa_{yy}))$ (s)	$\mathrm{mx}(\kappa_{yy})$ (m^2/s)	κ_{yy}^{∞} (m^2/s)	$t'(\kappa_{xx} > \kappa_{yy})$ (s)	$t'(\sigma_{xx} > \sigma_{yy})$ (s)
117	74	6.1 ± 0.5	2.2 ± 0.8	100	3.9 ± 0.3	3.8 ± 1.0	<140	<264
124	74	5.6 ± 0.4	1.3 ± 0.7	78	3.6 ± 0.3	2.8 ± 0.7	<170	<370
125	50	5.4 ± 0.6	0.9 ± 1.0	66	3.7 ± 0.4	3.8 ± 1.6	<94	<180
127	82	4.9 ± 0.4	1.9 ± 0.8	100	3.3 ± 0.3	3.9 ± 1.0	<154	<288
130	84	3.7 ± 0.3	2.5 ± 0.8	na	na	12.6 ± 2.4	<16	<30
135	96	2.6 ± 0.2	1.2 ± 0.5	na	na	2.4 ± 0.6	<164	<286
139	86	2.8 ± 0.2	0.1 ± 0.2	na	na	2.7 ± 0.4	<160	<274

[a]Here $t(\mathrm{mx}(\kappa_{xx}))$ and $t(\mathrm{mx}(\kappa_{yy}))$ are the time of maximum cross-shore and alongshore absolute diffusivity, respectively; $\mathrm{mx}(\kappa_{xx})$ and $\mathrm{mx}(\kappa_{yy})$ are the maximum cross-shore and alongshore absolute diffusivity, respectively; κ_{xx}^{∞} and κ_{yy}^{∞} are the asymptotic cross-shore and alongshore absolute diffusivity, respectively; $t(\kappa_{xx} > \kappa_{yy})$ is the time of greater cross-shore absolute diffusivity; and $t(\sigma_{xx} > \sigma_{yy})$ is the time of greater cross-shore patch spread. Absolute diffusivity (κ) values are $\pm\delta$ (sampling error).

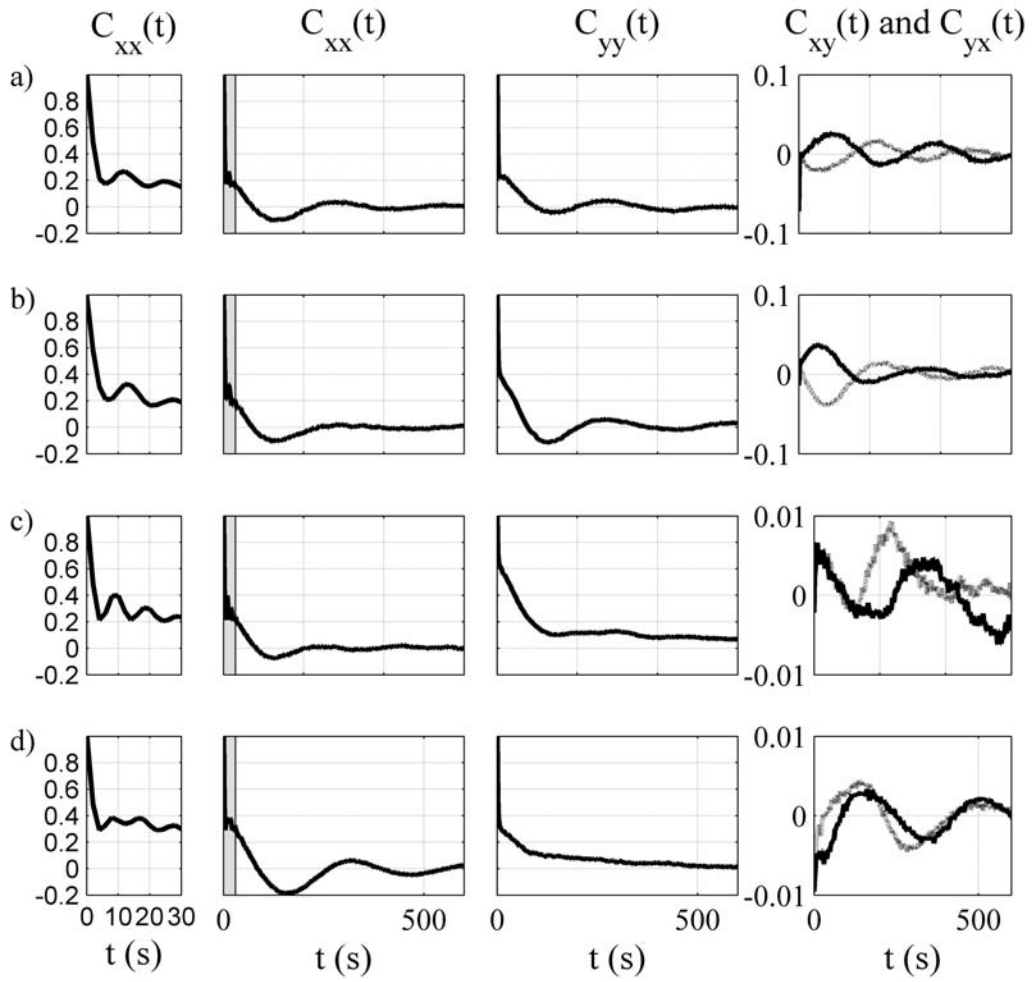

Figure 3. The (b, f, j, and n) cross-shore (C_{xx}) and (c, g, k, and o) alongshore (C_{yy}) anomalous Lagrangian velocity autocovariance plots for yeardays 117 (Figures 3a–3d), 124 (Figures 3e–3h), 130 (Figures 3i–3l), and 139 (Figures 3m–3p). (a, e, i, and m) Enlargements of the shaded portion of C_{xx}. (d, h, l, and p) The anomalous Lagrangian velocity cross covariances are plotted.

equivalent to (2) above where $i, j = x, y$ and $x_i(t')$ represents particle displacement from its initial position after time t' and the angle brackets represent ensemble averaging for all particle displacements at that time step [*LaCasce and Bower*, 2000].

[17] For an inhomogeneous velocity field, the diffusivity can also be calculated from the velocity covariance rather than the particle displacement variance, though using this method requires that modifications be made to (1) since κ becomes dependent upon particle starting position [*Davis*, 1987]. The drifter position is labeled with a second position ($\boldsymbol{x} = (\Delta \boldsymbol{x}, \Delta \boldsymbol{y})$) indicating the bin where it originated, so $\boldsymbol{r}(t'|\boldsymbol{x})$ is the displacement of the drifter t' seconds after it was in $\boldsymbol{x}$. Similarly, a drifter velocity is calculated as $\boldsymbol{v}(t'|\boldsymbol{x}) = d\boldsymbol{r}(t'|\boldsymbol{x})/dt'$. For a given bin $\boldsymbol{x}$, a time series of displacements $\boldsymbol{r}(t' = 0, 2, 4, 6, \ldots \text{s}|\boldsymbol{x})$ can be calculated for each drifter entering the bin. If a drifter reenters a bin, a new time series of displacements is calculated starting at the time of the drifter reentry. Similar to the pdf calculation, multiple time series of position displacements are obtained by incrementing the starting time and subtracting off the new initial position from the remaining measurements as long as the drifter position at t'_0 falls within bin $\boldsymbol{x}$. The average of all these tracks yields a mean drifter displacement $\boldsymbol{R}(t'|\boldsymbol{x})$, from which a mean drifter velocity is calculated, $\boldsymbol{V}(t'|\boldsymbol{x}) = d\boldsymbol{R}(t'|\boldsymbol{x})/dt'$. Relative velocity variations can be calculated, $v_i'(t'|\boldsymbol{x}) = v_i(t'|\boldsymbol{x}) - V_i(t'|\boldsymbol{x})$, which are used to calculate the spatially dependent anomalous Lagrangian velocity auto (cross) covariances

$$C_{ij}(\tau|\boldsymbol{x}) = \left\langle v_i'(t' = 0|\boldsymbol{x}) v_j'(t' = \tau|\boldsymbol{x}) \right\rangle, \tag{4}$$

where $i, j = x, y$ (includes cross terms) [*Spydell et al.*, 2007]. Angle brackets denote averaging over all values at separation τ = 0, 2, 4 … s, the time difference between velocity measurements. An unbiased estimate is obtained by making the number of observations at each τ equal to the number of observations at $\tau = 0$ s. Note that a biased estimate is similar to the unbiased estimate, but the unbiased estimate is used so that comparisons to *Spydell et al.* [2007] can be made.

[18] Since 90% of the drifters remain within the surf zone (Table 1) [*MacMahan et al.*, 2009a], all drifter deployments

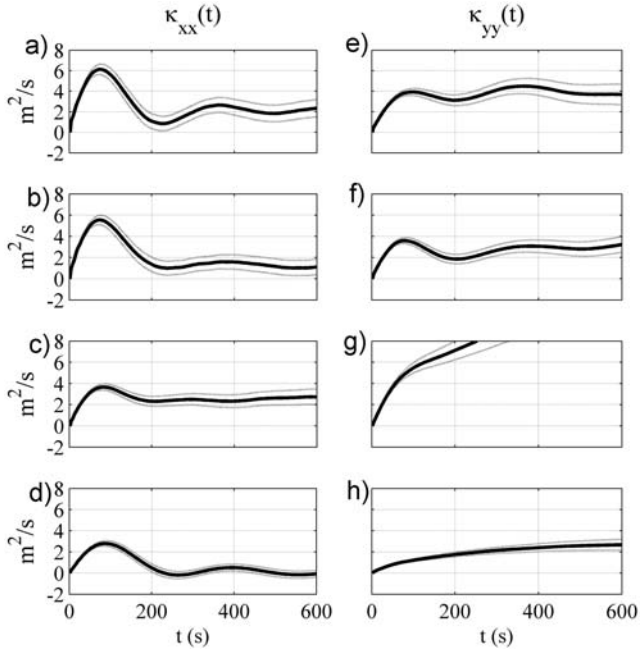

Figure 4. Absolute diffusivity (one particle) statistics ((a–d) κ_{xx} and (e–h) κ_{yy}) plotted with sampling error bounds $\delta(t)$ (gray lines) against time for yeardays 117 (Figures 4a and 4e), 124 (Figures 4b and 4f), 130 (Figures 4c and 4g), and 139 (Figures 4d and 4h). Here κ_{yy} = 12.5 m^2/s at t = 600 s for yearday 130 (Figure 4g).

are assumed to start in bin $\boldsymbol{x}$, the surf zone. The autocovariance functions are similar in shape for all days, but vary in magnitude (Figure 3). The variances are larger for rip current flows ($\sim$0.5 m^2/s^2 in the cross shore, $\sim$0.2 m^2/s^2 in the alongshore at τ = 0) versus the non rip current flows ($\sim$0.2 m^2/s^2 in the cross shore, $\sim$0.1 m^2/s^2 in the alongshore at τ = 0) due to larger velocities and more horizontal shear resulting from the rip currents and larger waves.

[19] Small amounts of periodic repetition are observed in C_{xx} (Figures 3a, 3e, 3i, and 3m) at τ = 12 s for yearday 117, 14 s for yearday 124, 10 s for yearday 130, and 8 s for yearday 139. These oscillations correspond to the peak wave period measured in 13 m water depth (Table 2).

[20] The largest oscillations correspond to a longer period ($\sim$300 s) that is observed for all days in C_{xx}. *LaCasce* [2008] provides a theoretical basis for a relationship between the covariance oscillations and the background motions influencing the drifters. The motion of a drifter can be simulated by a stochastic equation that includes a rotational element to mimic drifters that "loop" (for example, due to vortices). The introduction of the rotational element results in an autocovariance function that oscillates at the frequency of the rotational motion, a feature that has been demonstrated by real and simulated drifter deployments in coherent vortices in the North Atlantic. This also results in cross covariances (C_{xy}, C_{yx}) that oscillate with C_{xy} approximately equal and opposite to C_{yx}, i.e., 180° out of phase (Figures 3a–3h). For nonrotational elements, cross covariances are roughly equal and in phase [*Veneziani et al.*, 2004, 2005a, 2005b]. The oscillation period for RCEX is $\sim$300 s, corresponding to the observed average time for a particle to complete one revolution around the circulation cell [*MacMahan et al.*, 2009a]. While rip currents are not present for yearday 139, the drifters move in a sinuous alongshore fashion that behaves similar to a rotational motion in terms of cross-shore position, resulting in similar, though less pronounced, oscillations in C_{xx}. Alongshore autocovariance functions have small oscillations $\sim$300 s from peak to peak, in C_{yy} for the rip current flow patterns (Figures 3a–3h). The lack of oscillations in C_{yy} for yearday 139 indicates the lack of a rotational element in the alongshore flows (Figures 3m–3p) [*Veneziani et al.*, 2004, 2005a, 2005b]. An oscillatory behavior is present in the sinuous flow cross covariances, but now C_{xy} is approximately equal to C_{yx} (Figures 3m–3p). The cross covariances are useful in discriminating between a rotational pattern, nonrotational pattern, and a sinuous pattern.

[21] The integration of the velocity covariance corresponds to absolute diffusivity

$$\kappa_{ij}(t'|\boldsymbol{x}) = \int_0^{t'} C_{ij}(\tau|\boldsymbol{x})d\tau, \tag{5}$$

with $i, j = x, y$ (includes cross terms). $\kappa_{ij}(t'|\boldsymbol{x})$ is equivalent to (1) and quantifies the rate of change in the variance of $P(r_x', r_y'; t')$. Since the drifters are mainly contained within the surf zone, a representative $\boldsymbol{\kappa}$ for the entire area is determined and the label $\boldsymbol{x}$ is dropped. The sampling error, $\delta(t)$, is computed (gray lines in Figure 4) to determine the effects of sampling errors in C_{ij} on the calculation of κ_{ij} [*Bendat and Piersol*, 2000; *Spydell et al.*, 2007]. Sampling errors in κ at each time t' are calculated by taking the convolution of the Lagrangian autocovariance functions. κ is used to calculate the position displacement variance from (1) as

$$\sigma_{ij}^2(t') = 2\int_0^{t} \kappa_{ij}(t')dt', \tag{6}$$

where σ_{xx}^2 and σ_{yy}^2 represent the cross- and alongshore variance in particle displacement and are equivalent to (2). The standard deviations, σ_{xx} and σ_{yy}, represent the cross- and alongshore length scales of the ensemble averaged patch size. The patch becomes circular when $\sigma_{xx} = \sigma_{yy}$.

[22] The behavior of κ_{xx} is similar for all flow patterns, rising quickly to a peak before decreasing to an asymptotic oscillation (Figures 4e and 4f). The magnitudes of the peaks vary with flow pattern and wave height, peaking between 5.4 and 6.1 m^2/s for the rip current flow patterns and between 2.8 and 4.9 m^2/s for the meandering and alongshore flow patterns when there are smaller velocities and less shear (Table 3). Asymptotic values are similar for all flow patterns, varying between 0.9–2.2 m^2/s for the rip current flow patterns and 0.1–2.5 m^2/s for the meandering and alongshore flow patterns. The presence of different flow patterns and changes in wave conditions cause differences in diffusivity, with smaller waves and shorter periods forcing smaller currents with less velocity shear generally leading to smaller peak diffusivity. Peaks in κ_{xx} occur at increments of $\sim$300 s corresponding to the oscillations in the autocovariance functions (Figure 3) and the circulation times of the rip circulation cells [*MacMahan et al.*, 2009a]. The quick growth of κ_{xx} for

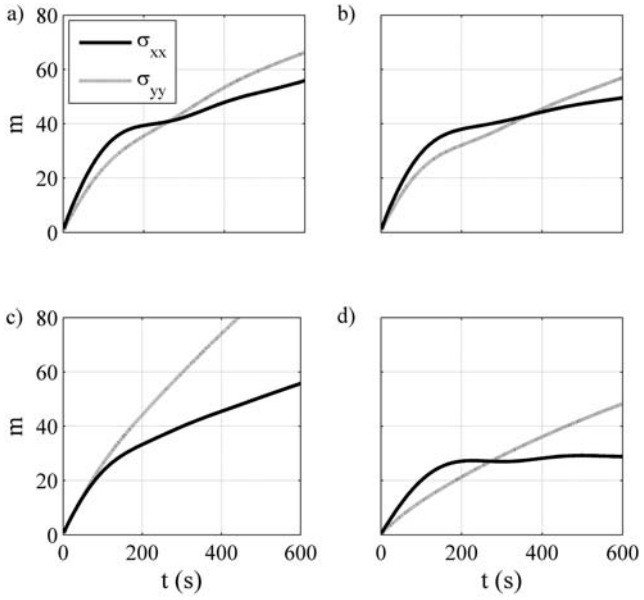

Figure 5. Plot of ensemble patch size area σ_{xx} (black line) and σ_{yy} (gray line) for yeardays (a) 117, (b) 124, (c) 130, and (d) 139.

$t' < 100$ s followed by a sharp decrease is reflected in early rapid growth in σ_{xx} followed by slower expansion (Figure 5). At the time of the initial peak in κ_{xx}, the cross-shore patch size $\sigma_{xx} \approx 25$ m, indicating that for a basically Gaussian distribution, 96% of the drifters are contained within $4\sigma_{xx} \approx 100$ m, roughly the cross-shore rip current dimension (within 15% difference), indicating the particles diffuse quickly until they span the entire surf zone at which time cross-shore diffusivity slows as particles oscillate between the seaward edge of the surf zone and the shoreline [*MacMahan et al.*, 2009a]. On yearday 139 the cross-shore absolute diffusivity, κ_{xx}, peaks at 2.8 m^2/s, then drops to near zero as cross-shore patch expansion stops almost completely after the initial dispersion (Figure 4).

[23] The values of κ_{yy} (Figures 4e–4h) are initially smaller but become larger than κ_{xx} for $t' > 170$ s. κ_{yy} either increases steadily until it reaches an asymptotic value for the rip current patterns (2.8–3.8 m^2/s), or increases to reach 2.4–12.6 m^2/s at $t' = 600$ s for the meandering and alongshore patterns. The large alongshore diffusivity for the meandering flow pattern is due to the nature of the flow field, where drifters varied between remaining in a single rip circulation cell and moving long distances alongshore, causing more deviation from the mean particle displacement and hence more diffusivity.

[24] High retention of drifters (~90%, Table 2) within the surf zone meant that in general there were insufficient measurements to calculate absolute diffusivity statistics for outside the surf zone. However, there were enough data on yeardays 117 and 124 with rip current flow patterns and the highest percentage of drifter exits for rip currents to obtain crude estimates of the absolute diffusivity outside the surf zone. The pixel intensities from time-averaged, rectified

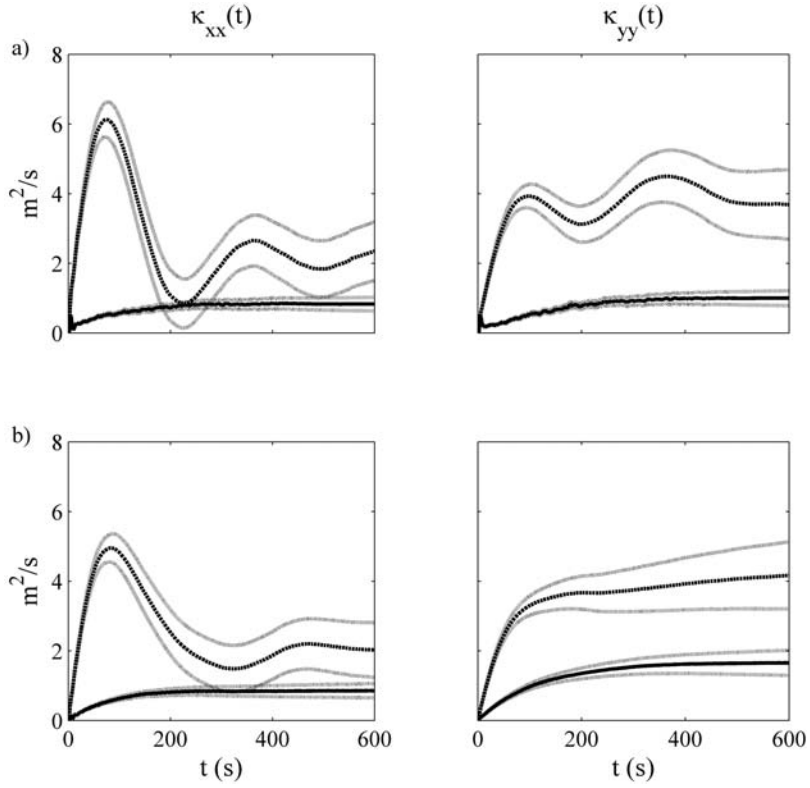

Figure 6. Absolute cross-shore, $k_{xx}(t)$, and alongshore, $k_{yy}(t)$, diffusivities for yeardays (a) 117 and (b) 124 calculated for outside (solid black lines) and inside (dotted black lines) the surf zone. The gray lines are 95% confidence intervals. The surf zone width was estimated from time-averaged rectified video images obtained during the drifter deployments [*MacMahan et al.*, 2009a].

Table 4. Two-Particle Relative Diffusivity[a]

Yearday	$t(D_{px} > D_{py})$ (s)	$\gamma_x(t = 10$ s)	$\gamma_y(t = 10$ s)	$t(\gamma_x = \gamma_y)$ (s)	γ	K_{px} (m^2/s)	K_{py} (m^2/s)	λ
117	<390	1.4	1.1	390	1.3	1.5–6.5	1.2–3.6	0.2
124	<290	1.4	1.2	280	1.3	1.5–6.4	1.5–3.9	0.1
125	<300	1.6	1.3	300	1.3	1.0–4.6	0.4–3.2	0.2
127	all t	1.2	1.0	580	1.3	1.2–4.6	0.8–3.0	0.2
130	<210	1.1	1.0	200	1.3	0.9–3.9	1.2–3.7	0.1
135	<200	1.0	0.8	190	1.3	0.4–2.7	1.1–2.2	0.1
139	<234	0.9	0.6	232	1.2	0.4–2.8	0.4–2.9	0.04

[a]Here $t(D_{px} > D_{py})$ is the time when the cross-shore relative dispersion is larger than alongshore relative dispersion; γ_x and γ_y are the cross- and alongshore γ values such that $D \sim t^{\gamma}$ at $t = 10$ s, respectively; $t(\gamma_x = \gamma_y))$ is the time when $\gamma_x = \gamma_y$ and γ is the associated value; and K_{px} and K_{py} are the cross- and alongshore relative diffusivities, respectively, with λ such that $K_p \sim d^{\lambda}$, where d is the separation. $D_{px} > D_{py}$, γ, and λ calculations are for the means across all initial separations.

video images were used to estimate the cross-shore position of the outer extent of the surf zone [*MacMahan et al.*, 2009a]. New deployments were created by dividing observations into two regions, inside and outside the surf zone. The absolute diffusivity was computed (equation (5)) for deployments outside the surf zone longer than 50 s.

[25] Asymptotic diffusivities computed outside the surf zone are smaller than those computed for the entire region for rip current flow patterns (Figure 6). The monotonic increase to an asymptote and lack of oscillations in the diffusivities indicate a lack of rotational structures outside the surf zone. Cross- and alongshore levels of diffusivity are similar outside the surf zone, suggesting isotropic particle spreading. Peak and asymptotic diffusivities inside the surf zone are slightly larger, and essentially the same as those computed over the entire region (Figure 4), peaking sharply before falling off to an oscillating asymptote. Higher diffusivity inside the surf zone reflects the contribution of shear and rotational elements to the total dispersive effects.

4. Relative Diffusivity: Two-Particle Statistics

[26] Two particle statistics describe the expansion of a cloud of particles in a frame of reference fixed to the cloud's center of mass measuring the change in the separation of the particles relative to each other. The relative dispersion, $D^2_{pi}(t', |\boldsymbol{s}_0|)$, represents the variance of $(s_i(t') - s_{0i})$ for all two-drifter separations for a deployment and is defined as

$$D^2_{pi}(t', |\boldsymbol{s}_0|) = \left\langle (s_i(t') - s_{0i})^2 \right\rangle - \langle (s_i(t') - s_{0i}) \rangle^2, \qquad (7)$$

with $i = x, y$ where angle brackets now denote ensemble averaging over all drifter tracks, s_i represents the separation between two drifters at time t', and s_{0i} is the initial separation at t'_0 [*Spydell et al.*, 2007]. Data are calculated as a function of initial separation magnitude, $|\boldsymbol{s}_0| = \sqrt{s^2_{0x} + s^2_{0y}}$, rather than $\boldsymbol{s}_0$ to simplify the interpretation while increasing the number of binned separations. Two-particle initial seperations, $|\boldsymbol{s}_0|$, are binned into 0–4 m, 4–8 m, 8–16 m, 16–32 m, and >32 m. Owing to the number of drifters deployed and their relatively long position time series, a maximum record length of 600 s is used. To increase the number of (not independent) separation estimates for two drifters that are simultaneously deployed for $t' > 600$ s, separations are computed at every temporal lag of 10 s. For example, if the drifters overlap for 800 s, an $\boldsymbol{s}_0$ and $\boldsymbol{s}_i(t')$ are calculated for $t' = 0–600$ s, then a new $\boldsymbol{s}_0$ and $\boldsymbol{s}_i(t')$ are calculated at $t' = 10–610$ s, until $t' = 200–800$ s, creating 20 additional 600 s separation records. Additional $\boldsymbol{s}_i(t')$ are computed for this pair, for $t' = 210–800$ s, 220–800 s, etc, until $t' = 750–800$ s, increasing the separation records by 55. So for 800 s of overlapped time for two drifters, 75 different (not independent) records are computed. This is repeated for all drifter pairs on a deployment day. Similar to the one-particle statistics, the two-particle statistics are estimated for the entire surf zone region.

[27] Dispersion magnitudes (Table 4) differ for different initial separations (Figure 7), but the trends are consistent. The dispersions are plotted with black lines representing $D^2 \sim t'^{\gamma}$ for $\gamma = 1$, 2 and 3 for comparison with $D^2 \sim t'^3$ [*Richardson*, 1926]. In general, the patches are initially elongated in the cross shore ($D^2_{px} > D^2_{py}$) before becoming circular ($t' = 200–400$ s) then alongshore elongated. The patch on yearday 130 was close to circular, only slightly alongshore polarized. The initial two particle separation is minimal for $|\boldsymbol{s}_0| \leq 4$ m and begins to increase after roughly one-half revolution (100–150 s), consistent with visual observations and dye comparisons [*MacMahan et al.*, 2009a, 2009b]. For small initial separations, the drifters initially travel along similar streamlines, subject to background diffusion before the shear induces larger dispersion.

[28] A power law relationship is sought for the average of all the initial separations as a function of t' in order to estimate $\gamma(t)$. For all yeardays, γ is initially larger for $D^2_{px} > D^2_{py}$ with $\gamma_x = 0.9–1.6$ and $\gamma_y = 0.6–1.3$ at $t' = 10$ s (Table 4). This reflects the faster spread in the cross shore, as seen in the absolute diffusivity. Initial values of γ_x are larger for the rip current flow patterns than the other patterns (Table 4) as a result of larger velocities and larger rotational shear from the motions. The rates of expansion become similar at larger t' (200–600 s) with $\gamma_x = \gamma_y \approx 4/3$ indicating a background level of diffusivity for all flow patterns, though differences occur from the presence of shear and differing wave conditions. *Spydell et al.* [2007] found $\gamma_x = \gamma_y \approx 3/2$ for a beach with relatively straight and parallel contours.

[29] Relative diffusivity, K_{pi}, is the rate of change in dispersion

$$K_{pi}(t', |\boldsymbol{s}_0|) = \frac{1}{4} \frac{d}{dt'} D^2_{pi}(t', |\boldsymbol{s}_0|), \qquad (8)$$

where the 1/4 is used because the separation of two particles is twice as large compared with the deviation of a particle

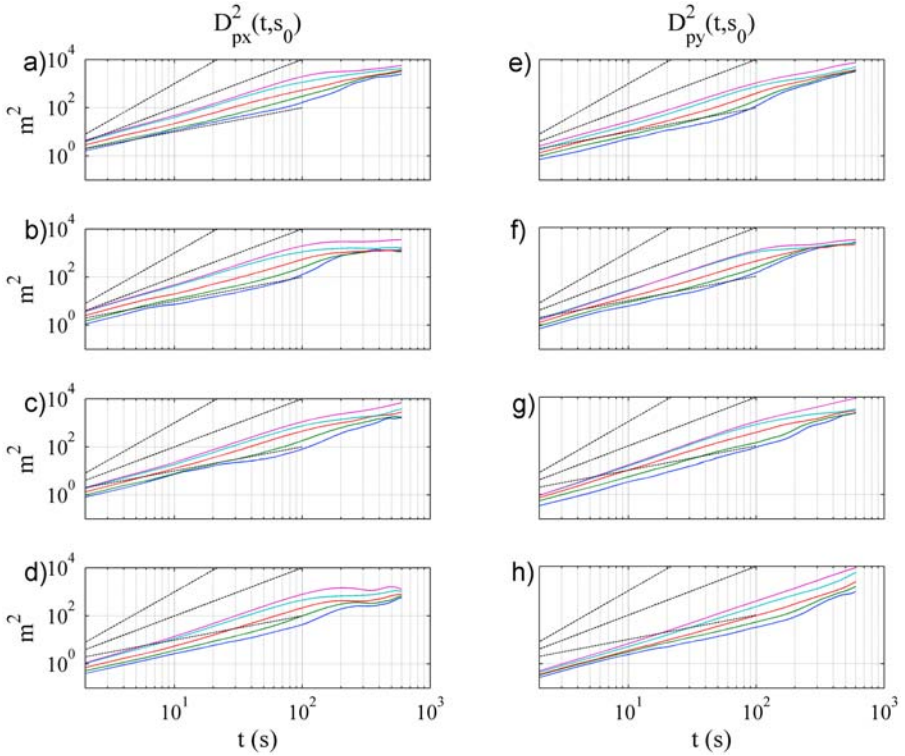

Figure 7. Representative relative dispersion (a–d) D^2_{px} and (e–h) D^2_{py} calculated from two-particle statistics for yeardays 117 (Figures 7a and 7e), 124 (Figures 7b and 7f), 130 (Figures 7c and 7g), and 139 (Figures 7d and 7h). The black lines represent $D^2 \sim t^\gamma$ for γ = 1, 2, and 3. The colors represent the different initial separation magnitudes, $|\boldsymbol{s}_0|$, of 0–4 (blue lines), 4–8 (green lines), 8–16 (red lines), 16–32 (cyan lines), and >32 m (magenta lines).

from the mean particle position, or $D^2_{pi} = 2\sigma^2_{ii}$. The relative diffusivity is plotted versus a measure of separation, d, where

$$d = \sqrt{D_{px}(t', |\mathbf{s}_0|) D_{py}(t', |\mathbf{s}_0|)} \tag{9}$$

is the radius of a circle with area equal to an ellipse with axes D_{px} and D_{py} [*Spydell et al.*, 2007] (Figure 8). The spatial growth of a patch is characterized by d because the original separation is removed from D and reflects the same spatial dependence as $K_p \sim l^\lambda$ (where $l = (d^2 + |\boldsymbol{s}_0|^2)^{1/2}$) [*Richardson*, 1926; *Spydell et al.*, 2007]. Values of K_{pi} are noisy due to the effects of the rotational motions for $t > 300$ s so only the initial 300 s are shown (Figure 8). K_{px} and K_{py} for the rip current patterns begin to decrease for $d > 25$ m as the particles reach a maximum separation and stop expanding as most of the drifters are retained within the surf zone. This decrease occurs in K_{px} but not K_{py} for the meandering and alongshore flow patterns (yeardays 130, 139, Figures 8c, 8d, 8g, and 8h) as the particles oscillate in the cross shore, but are not subjected to rotational flows in the alongshore, and the particles remain correlated as they moved alongshore. Estimates of K_{px} differ with initial separation but are generally larger for the rip current patterns, K_{px} = 1.0–6.5 m^2/s, than the meandering and alongshore flow patterns, K_{px} = 0.4–4.6 m^2/s, as the wave heights were generally lower and the surf zone velocities and velocity shear decreased. The values of K_{py} are consistently less than K_{px} for the rip current flow patterns, while K_{px} and K_{py} are similar for the other flow patterns with K_{py} = 0.4–3.7 m^2/s. The power law relationship $K_p \sim d^\lambda$ is only determined over the smaller scales due to the decorrelation of length scale and diffusivity for larger separations. The black lines represent $K_p \sim d^\lambda$ for λ = 1/10, 2/10 and 4/3. For all days the relationship is weaker than Richardson-like, $K_p \sim d^{4/3}$, with $\lambda \approx 0.2$ for the rip current patterns and $\lambda \approx 0.1$ for the wandering and alongshore flow patterns.

5. Relative Diffusivity: Cluster Statistics

5.1. Horizontal Eddy Diffusivity

[30] The formulation for absolute (one particle) and relative (two particle) diffusivities assumes that the flow field is stationary to compute representative statistics across the surf zone and that all drifters are subjected to the same motions, making them members of a "cluster" regardless of deployment time or location. The two-particle computation infers an estimate of the centroid. If drifters are originally deployed in clusters, a "true" centroid is determined at each time step by the mean location of all the drifters and the separation from the centroid is used to estimate relative diffusivity, K_e (analogous with K_p). For this discussion, a cluster is defined as a set of n drifters (n $\geq$ 4) that are released from a common location and are active in the surf zone for $t \geq 590$ s. Diffusivity estimates are computed from the time that the cluster is released until the first drifter is removed from the surf zone. Table 5 summarizes the cluster releases for the drifter deployments that met these criteria.

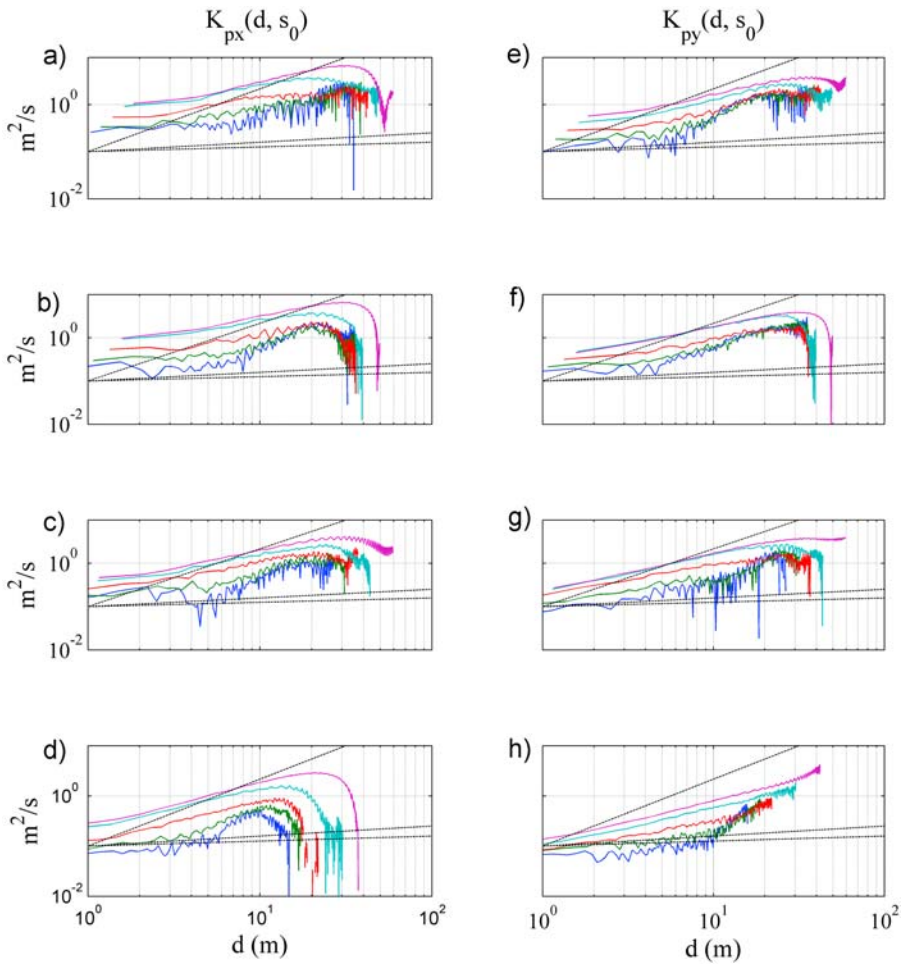

Figure 8. Relative diffusivity (two particle) ((a–d) K_{px} and (e–h) K_{py}) plotted versus separation d for yeardays 117 (Figures 8a and 8e), 124 (Figures 8b and 8f), 130 (Figures 8c and 8g), and 139 (Figures 8d and 8h). Black lines represent $K_p \sim d^{\lambda}$ for λ = 1/10, 2/10, and 4/3. Colors represent different initial separation magnitudes as used in Figure 7.

[31] An effective diffusion coefficient (relative diffusivity) for a cluster is defined as

$$K_e = K_{ex} + K_{ey} = \frac{1}{2}\frac{dD_{ex}^2}{dt} + \frac{1}{2}\frac{dD_{ey}^2}{dt} = \frac{1}{2}\frac{d\left(D_e^2\right)}{dt}, \qquad (10)$$

where the sum of the directional diffusion coefficients characterizes the spread of the patch (Table 5), with the cross-shore and alongshore dispersions calculated as

$$\left(D_{ex}^2, D_{ey}^2\right) = \frac{1}{n-1}\left(\sum_1^n \left(x_i'\right)^2, \sum_1^n \left(y_i'\right)^2\right), \qquad (11)$$

where x'_i and y'_i are the horizontal displacements of the ith drifter from the cluster centroid (modified from *Drinkwater and Loder* [2001], *Johnson and Pattiaratchi* [2004], and *List et al.* [1990]). The 1/2 is used here because the calculations of displacement are relative to a centroid, similar to the absolute dispersion. These definitions of cluster dispersion and diffusion are chosen to allow comparisons between two-particle and clusters statistics and to present a rational for reconciling the different definitions of cluster diffusivity in the literature [*Smith*, 1989; *List et al.*, 1990; *Drinkwater and Loder*, 2001; *Johnson and Pattiaratchi*, 2004; *Manning and Churchill*, 2006].

[32] The patch location and size, an ellipse with axis D_{ex} in the cross shore and D_{ey} in the alongshore, are plotted with D_e, D_{ex}, and D_{ey} (Figure 9) for a single deployment on a rip current flow pattern day (yearday 124, deployment 5) to show the patch behavior as a function of location within the rip current. Dispersion is larger in the cross shore, when the cluster is in the rip channel or over the shoal. Dispersion is more circular and/or alongshore polarized when the centroid is traveling in the alongshore. Initially, dispersion (t < 70 s) is small as the drifters move along similar streamlines before shear effects become dominant (discussed below), similar to the behavior of the two-particle pairs for small initial separation. The patch then (t < 150 s) is stretched in the cross shore and contracts in the alongshore due to focusing within the rip channel. The flow of a rip current acts as a solid body of rotation, as the patch in the rip channel is rotated across the top of the rip current cell (t > 150 s), the elongated cross-shore axis of the patch in the rip channel becomes the alongshore

Table 5. Cluster Relative Diffusivity and Turbulent Eddy Diffusivity[a]

Deployment	Number of Drifters	Deployment Duration (s)	K_e (m^2/s)	k_{xy} (m^2/s)	k'_{xy} (m^2/s)
		Yearday 117			
1	4	1100	1.2	–	
2	10	590	1.2	0.4	
3	6	1100	3.2	0.4	
4	10	1014	7.8	0.6	
5	6	746	4.4	0.5	
mean			3.6	0.5	0.5
		Yearday 124			
1	8	1700	1.6	0.4	
2	5	610	6.3	0.2	
3	8	730	2.3	0.3	
4	5	970	1.1	0.2	
5	8	770	0.83	0.3	
6	4	790	0.77	–	
mean			2.2	0.3	0.3
		Yearday 125			
1	9	980	1.5	0.6	
2	10	1300	1.9	0.6	
mean			1.7	0.6	0.5
		Yearday 127			
1	4	880	7.2	–	
2	8	660	3.9	0.2	
3	6	890	2.5	0.2	
mean			4.5	0.2	0.3
		Yearday 130			
1	9	2200	3.2	0.2	
2	6	600	1.4	0.2	
3	5	610	4.6	0.1	
4	6	870	2.9	0.2	
mean			3.0	0.2	0.2
		Yearday 135			
1	10	740	5.1	0.1	
2	10	590	1.7	0.2	
3	6	1200	1.2	0.1	
4	7	600	3.7	0.1	
mean			2.9	0.1	0.2
		Yearday 139			
1	8	650	0.9	0.03	
2	6	890	2.0	0.1	
3	10	850	1.0	0.1	
4	9	690	0.7	0.1	
5	10	600	0.6	0.1	
6	7	910	1.0	0.1	
7	5	980	1.0	0.1	
mean			1.0	0.1	0.1

[a]Here K_e is the relative diffusivity calculated with clusters, k_{xy} is the turbulent eddy diffusivity, and k'_{xy} is the turbulent eddy diffusivity.

axis. This action plus shear in the alongshore spreads the patch in the alongshore. The elongated patch results in oscillation in K_{ex} and K_{ey}. Note that the travel times are specific to this particular deployment as the location within the rip is dependent on deployment locations and flow patterns, though the general trends in cluster behavior remain the same.

[33] Owing to the noise in instantaneous diffusion coefficients K_e, K_{ex}, and K_{ey}, cluster behaviors are analyzed from the less noisy dispersions, D_e^2, D_{ex}^2, and D_{ey}^2. Smoothed K_e, K_{ex} and K_{ey} values are calculated from the dispersion slopes for different temporal segments (Figure 10) of the clusters' evolution [*Johnson and Pattiaratchi*, 2004]. For all days, initial cluster dispersion ($t < 70-300$ s) is minimal as the drifters move in similar streamlines until the background dispersion separates the particles enough for the shear to take effect. Negative values of K_e indicate that the drifters in a cluster are contracting rather then expanding. A total mean horizontal diffusion coefficient is determined by taking the mean of the instantaneous K_e for the whole deployment.

[34] The average K_e is $\sim$1.2 m^2/s for the rip current days shown (yearday 117, deployment 2 and yearday 124, deployment 4; Figures 10a and 10b). Total mean horizontal diffusion varies with deployment due to the fact that a cluster deployment represents an instantaneous measurement. The average diffusion for all clusters on rip current days is 2.5 m^2/s (Table 5), larger than the two deployments shown. For rip currents, both D_{ex} and D_{ey} oscillate initially at $\sim$25 m, altering the cluster spread in the cross-shore and alongshore directions, but without causing much total dispersion (Figure 9). This oscillation about 25 m is similar for D_{ex} cluster calculations for the alongshore current pattern. The surf zone width, $\sim$100 m, is roughly four times the asymptote of D_{ex} similar to the patch size determined earlier from the absolute diffusivity and dispersion, confirming that most particles are contained within one surf zone width, consistent with the observed lack of drifter exits from the surf zone [*MacMahan et al.*, 2009a].

[35] The mean diffusivity for the meandering flow pattern (yearday 130, deployment 4) is similar, with a mean of

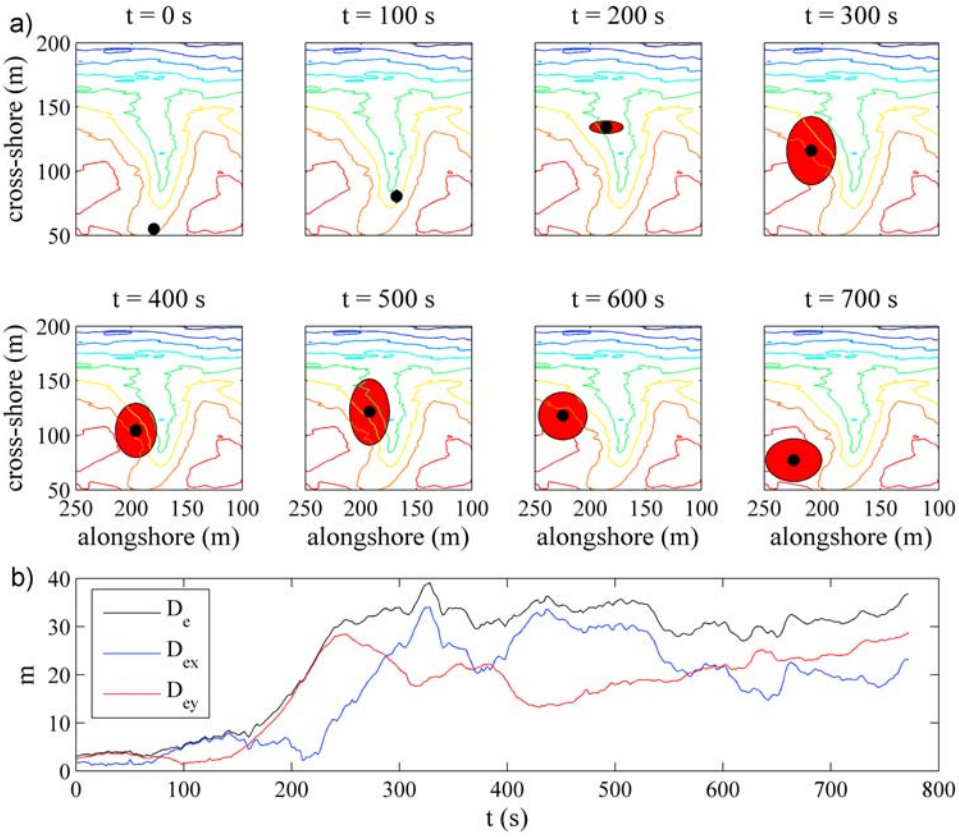

Figure 9. (a) Centroid location (black circle) and cluster size (red ellipse) at 100 s time steps plotted on top of the bathymetry for yearday 124, deployment 5 (Table 4). (b) The cluster patch sizes ($D_e = D_{ex} + D_{ey}$, D_{ex}, and D_{ey}) are plotted corresponding to the ellipse (axis defined by D_{ex} in the cross shore and D_{ey} in the alongshore) plotted in Figure 9a. The drifter cluster remained predominantly in one rip current cell for this deployment.

3.0 m^2/s for the deployment shown (Figure 10c) and 3.0 m^2/s for all deployments on the day (Table 5). There are no rip current circulation cells to contain the cluster so expansion measured by D_{ex}^2 and D_{ey}^2 are not subject to the contraction and expansion induced by the rip current flow patterns.

[36] The cross-shore dispersion for the cluster deployed in the sinuous alongshore flow pattern (yearday 139, deployment 2, Figure 10d) exhibits similar behavior to the rip current pattern, quickly spreading then oscillating in D_{ex} with a steadily increasing D_{ey} that exhibits none of the oscillations present with rip current patterns. The steady increase in D_{ey} results from the lack of a rotational element in the alongshore flow.

5.2. Comparison of Cluster and Two-Particle Statistics

[37] In general, previous studies have focused their analysis of drifter behaviors on either particle statistics or cluster statistics based on the constraints of their deployments. Particle statistics require a number of drifters (>5) (not necessarily deployed at the same instant in time), while cluster statistics require a number of drifters (>5) that are deployed at the same time. The drifter deployments for RCEX satisfy both requirements. A comparison is made between the diffusivity calculated from the cluster method and two particle statistic method. The two-particle method quantifies the spread of particles relative to each other while the cluster statistics measure variance from a group centroid, which should be equivalent [*LaCasce*, 2008]. To compare K_e with K_p, a total $D_s^2(t, \boldsymbol{s}_0)$ is calculated as

$$D_s^2(t, \boldsymbol{s}_0) = D_{px}^2(t, \boldsymbol{s}_0) + D_{py}^2(t, \boldsymbol{s}_0), \tag{12}$$

where D_{px}^2 and D_{py}^2 are determined by applying the two-particle statistic methodology (section 4) to the drifters in a particular group rather than the entire day. K_e and K_p are one-half and one-fourth the derivatives of D_e^2 and D_s^2, respectively, so their relationship can be evaluated by comparing D_e^2 with $1/2D_s^2$, which are less noisy. D_e^2 is compared to $1/2D_s^2(t, \boldsymbol{s}_0 = 4\text{ m})$ due to the proximity of the drifters to each other when the group is deployed. D_s and D_e are significantly correlated ($R^2 > 0.9$) at 95% confidence intervals (Table 6) with the smoother curve of D_s following the noisier trends of D_e (Figure 11). The trend of D_s is smoother due to averaging over a large number of drifter pair separations while the calculation of D_e represents a single instance of cluster spreading. The significant correlation between the two methods suggests that both methods are equivalent, as suggested by *LaCasce* [2008], even in a nonhomogeneous flow field. This suggests that the behavior of a cluster of

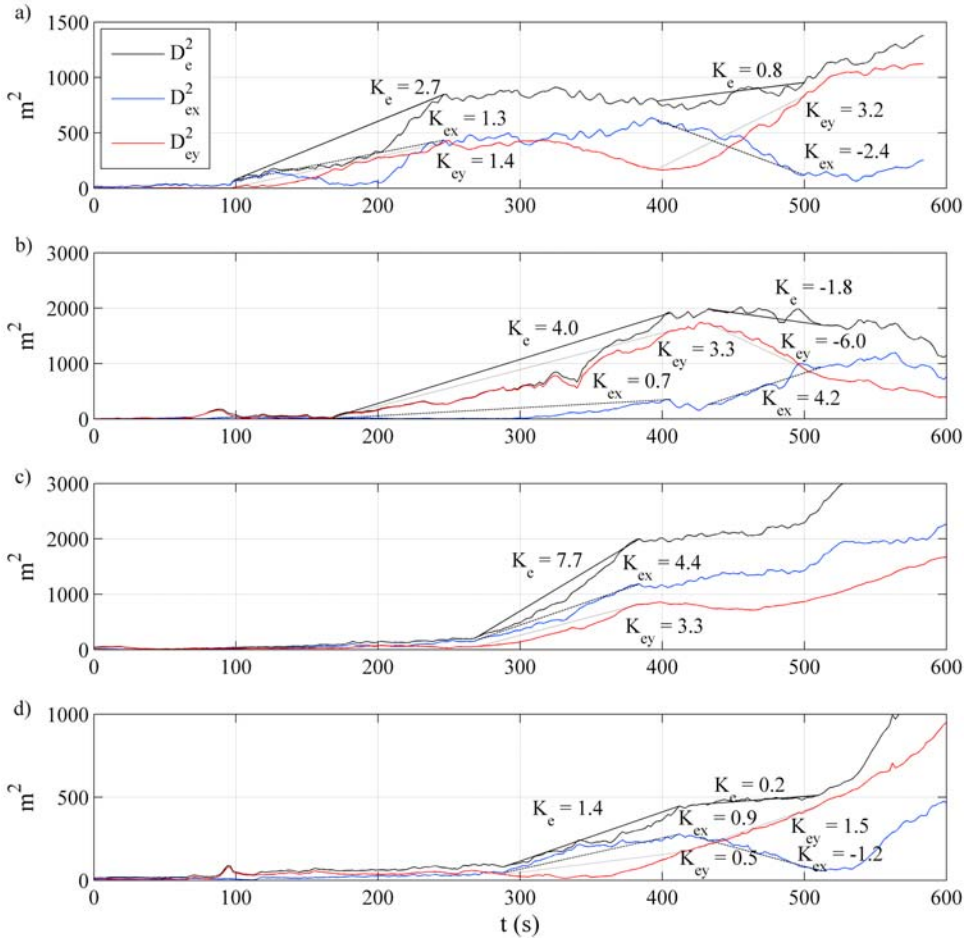

Figure 10. Total (black line), cross-shore (blue line), and alongshore (red line) squared patch size for a representative cluster from (a) yearday 117, deployment 2; (b) yearday 124, deployment 4; (c) yearday 130, deployment 4; and (d) yearday 139, deployment 2 (Table 4). Values of the horizontal diffusion coefficients (K_e, K_{ex}, and K_{ey} with units of m^2/s) are calculated at different places in the temporal evolution of the cluster to illustrate variation in alongshore and cross-shore diffusivity measurements.

particles is representative of the typical diffusion for a region, even if large numbers of drifters were not simultaneously released. Note there is no correlation between the number of drifters in a cluster and the correlation between the two relative diffusivity statistics (two particle and cluster). The suggested number of drifters in a cluster needed to accurately quantify the diffusivity is at least 5 [*Okubo and Ebbesmeyer*, 1976] but this was not verified. Despite similarities in dispersion and diffusion estimates using the two methods, there is benefit in observing the group deployments, which display some drifter behaviors that are smoothed out by the averaging of the two-particle statistics.

6. Small-Scale Turbulent Diffusivity

6.1. Separating Small-Scale Turbulent Diffusivity

[38] The objective is to separate the small-scale turbulent diffusivities from the larger-scale processes. It is hypothesized that the small-scale turbulence is produced by the dissipation of the breaking waves and therefore has length and time scales on the order of the breaking waves. The space and time separations of the small-scale turbulent processes from the large-scale processes are accomplished using two independent methods that are shown to give similar results.

[39] The first method is a two step process. First, the observations of a cluster of drifters ($\geq$4 drifters) are used to differentiate the longer length scales of the mean shear flow contributions to the diffusivity from the smaller length scales of the background turbulent flow components [*Okubo and Ebbesmeyer*, 1976]. Expanding the velocities at a particular time t of the ith drifter in a Taylor series,

$$u_i(t) = \overline{u}(t) + \frac{\partial \overline{u}(t)}{\partial x} x_i(t) + \frac{\partial \overline{u}(t)}{\partial y} y_i(t) + u_i''(t)$$
$$v_i(t) = \overline{v}(t) + \frac{\partial \overline{v}(t)}{\partial x} x_i(t) + \frac{\partial \overline{v}(t)}{\partial y} y_i(t) + v_i''(t), \quad (13)$$

Table 6. Correlation Between Two-Particle and Cluster Diffusivity[a]

Yearday	Deployment	R^2	m	b
117	2	0.95	1.21	13.3
124	4	0.98	0.74	104.1
130	4	0.98	0.78	25.3
139	2	0.96	1.06	80.5

[a]Here R^2 is the correlation coefficient, m is the slope of best fit line, and b is the y intercept of best fit line. Data is O(10^3).

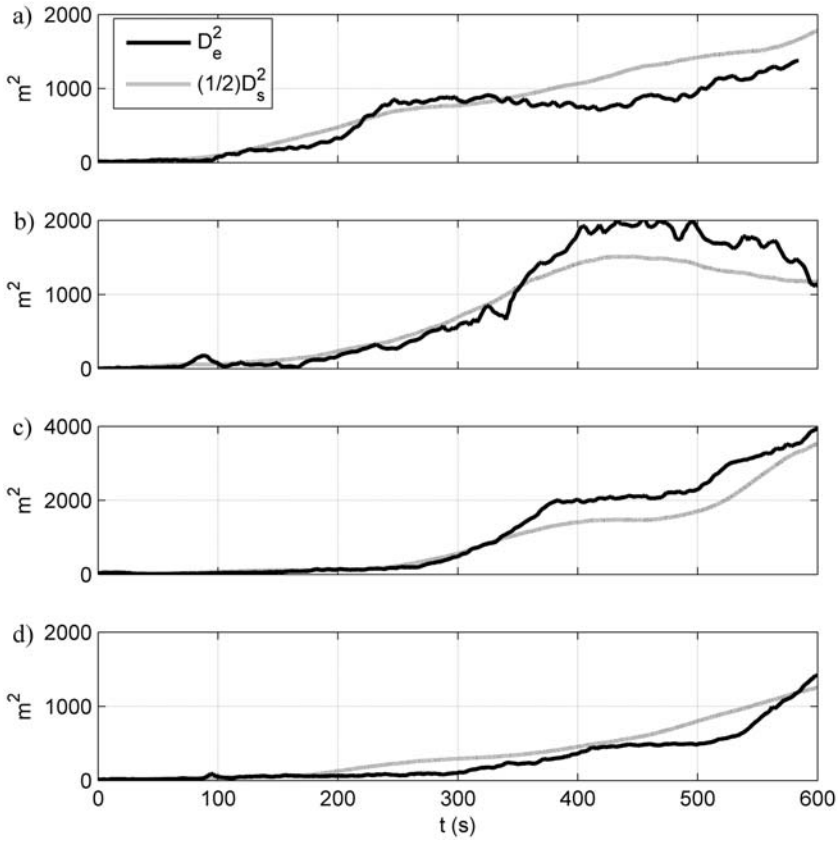

Figure 11. The total relative dispersion resulting from performing the two particle statistics analysis on the cluster for particles initially separated by less than 4 m, D_s^2 (t, 4 m) (gray line), and the total displacement of the cluster, D_e^2 (black line), for the clusters shown previously for yeardays (a) 117, (b) 124, (c) 130, and (d) 139.

where u_i, v_i are the drifter velocity components in the x, y directions relative to the centroid, $\overline{u}$, $\overline{v}$ are the ensemble mean velocities of the centroid at time t, and u''_i, v''_i indicate the velocity residuals, assumed to represent turbulence, but may include also higher-order terms and errors [*Okubo and Ebbesmeyer*, 1976]. The four unknowns in (12) can be solved when the number (n) of drifters ≥ 4, providing four independent equations for all times t in each cluster deployment. In practice, $n \geq 5$ is required to have enough degrees of freedom and only deployments with at least 5 drifters are considered. This equation set is solved by minimizing the sum of the residuals squared to solve for the unknown mean velocity shears and gradients. It is assumed the higher-order terms in the Taylor series expansion are negligible and the errors are small so that the velocity residuals represent the turbulent flow components to diffusivity with the mean velocity and velocity shears removed.

[40] Next, the method suggested by *List et al.* [1990] is used to separate time scales. This technique is analogous to time splitting in numerical turbulence models where advection and diffusion are solved separately at each time step. Expressing the turbulent velocities obtained using (13) in a forward time stepping of the drifter displacements

$$u_i''(t) = \frac{x(t+\Delta t) - x(t)}{\Delta t}; \quad v_i''(t) = \frac{y(t+\Delta t) - y(t)}{\Delta t}. \tag{14}$$

Solving for the turbulent diffusivities

$$k_x(t) = \frac{1}{2}\frac{\left[\sigma_x^2(t+\Delta t) - \sigma_x^2(t)\right]}{\Delta t}; \; k_y(t) = \frac{1}{2}\frac{\left[\sigma_y^2(t+\Delta t) - \sigma_y^2(t)\right]}{\Delta t}, \tag{15}$$

where the dispersion of the drifters positions at times t and $t + \Delta t$ are solved from (14). The turbulent eddy diffusivity is calculated as

$$k_{xy}(t) = k_x(t) + k_y(t), \tag{16}$$

with the cross-shore and alongshore components of turbulent diffusivities given by

$$k_i(t) = \frac{\langle u''\rangle^2(t)\Delta t}{2} + \overline{x_i'(t)u_i''(t)}, \quad k_y(t) = \frac{\langle v''\rangle^2(t)\Delta t}{2} + \overline{y_i'(t)v_i''(t)}, \tag{17}$$

where i denotes the drifter, x_i' and y_i' represent the distance of the drifter i from the cluster centroid and the overbar is the

average. The turbulent intensity components are calculated from the velocity residuals as

$$(\langle u'' \rangle, \langle v'' \rangle) = \left[\frac{1}{n-1} \left(\sum_1^n \left(u_i''\right)^2, \sum_1^n \left(v_i''\right)^2 \right) \right]^{1/2}, \quad (18)$$

where $\langle\ \rangle$ denotes ensemble value. Values computed for k_{xy} range 0.1–0.6 m^2/s (Table 5).

[41] The second method uses the autocovariance function to obtain diffusivity of the small-scale turbulence. Assuming weak nonlinearities such that motions at different length and time scales are independent, the autocovariance function can be characterized as the summation of individual autocovariance functions for motions at separated scales composed of contributions from mean currents and rip currents, sea swell waves, and background turbulence. Since the drifters only measure surface currents, only horizontal turbulent eddies (vortices) with axis in the vertical plane are considered. If the turbulence is characterized as white noise, the autocovariance function is a delta function that decorrelates within one temporal (spatial) lag [*Bendat and Piersol*, 2000]. A spike is observed in the autocovariance functions between $\tau = 0$ and $\tau = \Delta$t (Figures 3a, 3e, 3i, and 3m), which is hypothesized to represent the background turbulence. The eddy diffusivity can be estimated as the area of the delta function contribution to the autocovariance function

$$\kappa'_{xx} \approx [C_{xx}(\tau = 0|x) - C_{xx}(\tau = \Delta t)|x)]\Delta t, \quad (19)$$

with k'_{yy} found similarly from C_{yy}, and $k'_{xy} = k'_{xx} + k'_{yy}$. Values of k'_{xy} range 0.1 to 0.6 (Table 5), similar to values of k_{xy}. k_{xy} and k'_{xy} are found to be significantly correlated (R^2 = 0.9, slope = 1.3, y intercept = −0.1) at the 95% confidence level.

6.2. Turbulent Eddy Diffusion Generated by Breaking Waves

[42] *Battjes* [1975], assuming straight and parallel bottom contours, used an energy balance ($\frac{dEc_{gx}}{dx} = \varepsilon_b$) to solve for the turbulent eddy diffusion by assuming that the production of turbulence generated by breaking waves is equal to the vertically averaged dissipation per unit area, ε_b, where E is wave energy and the group velocity in the x direction $c_{gx} \approx c_g$ for the assumed normally incident waves. The turbulent eddy viscosity is given by

$$\upsilon_t = \alpha H \left(\frac{\varepsilon_b}{\rho} \right)^{1/3}, \quad (20)$$

where ρ is density of seawater, with the scale of the turbulence given by the incident wave height, H, representing a mixing length, and α is a calibration factor of O(1).

[43] Neglecting wave reflection or transfer of energy to lower-frequency waves, all incident wave energy is dissipated by wave breaking within the surf zone, and the surf zone-averaged wave energy dissipation, $\overline{\varepsilon}_b$, can be obtained from the wave energy balance by integrating across the surf zone width, X_S, yielding

$$\overline{\varepsilon}_b = \frac{1}{X_S} \int_{X_s}^{0} \frac{dEc_g}{dx}\, dx = \frac{(Ec_g)_0 - (Ec_g)_{X_s}}{X_S}, \quad (21)$$

which states that the mean production and dissipation of turbulent energy integrated over the surf zone are in balance [*Battjes*, 1975]. Outside the surf zone, the incident energy flux is constant and can therefore be evaluated with the measurements obtained at 13 m depth (Table 2) whereas the energy flux at the shore line, $x = X_S$, equals zero assuming no energy passes into the swash zone landward of $h = 0$. Hence, the surf zone averaged wave energy dissipation is calculated by

$$\overline{\varepsilon}_b = \frac{(Ec_g)_{x|h=-13m}}{X_s}, \quad (22)$$

with the incident wave energy in 13 m given by

$$E = \frac{1}{16} \rho g H_s^2, \quad (23)$$

where H_s is the significant wave height and the group velocity is obtained from linear wave theory:

$$c_g = \left(\frac{1}{2} + \frac{kh}{\sinh(2kh)} \right) \frac{\omega}{k}, \quad (24)$$

where $\omega = \frac{2\pi}{T_p}$ with T_p as the period of the peak of the wave spectrum and the wave number k is obtained from the linear dispersion relation

$$\omega^2 = gk \tanh kh. \quad (25)$$

Values for the surf zone averaged wave-breaking induced turbulent eddy viscosity, υ_t, are calculated using the values given for waves in 13 m water depth and X_S (Table 2). Values of the estimated small-scale turbulent diffusivities (k_{xy}, k'_{xy}) are compared with calculated breaking wave induced υ_t values using an optimized constant value for $\alpha = 0.7$ in (20) and both were found to be significantly correlated at the 95% confidence interval (R^2 = 0.95) (Figure 12).

7. Discussion

7.1. Surf Zone Diffusivity Comparisons

[44] The cross-shore absolute diffusivity κ_{xx} asymptotes measured here (0.9–2.2 m^2/s) on days with rip current flow patterns are similar in magnitude to earlier dye measurements on a beach with rip currents (0.08–5.9 m^2/s), but alongshore absolute diffusivities κ_{yy} measured here (2.8–3.8 m^2/s) are an order of magnitude larger than the 0.03–0.2 m^2/s measured by *Inman et al.* [1971]. Absolute diffusion in the rip current flow patterns is initially dominated by the cross shore, as found by *Inman et al.* [1971], but for large t the diffusion becomes alongshore dominated similar to *Johnson and Pattiaratchi* [2004]. The large initial diffusivity followed by a sharp decline results from the expansion and contraction, as the particles are quickly dispersed initially then begin to regroup, slowing the spread.

[45] For the sinuous alongshore flow field, which more closely represents the conditions observed by *Spydell et al.* [2007], the alongshore diffusivities measured here are similar in magnitude (2.7 m^2/s) to theirs (2.0–4.5 m^2/s). Initial cross-

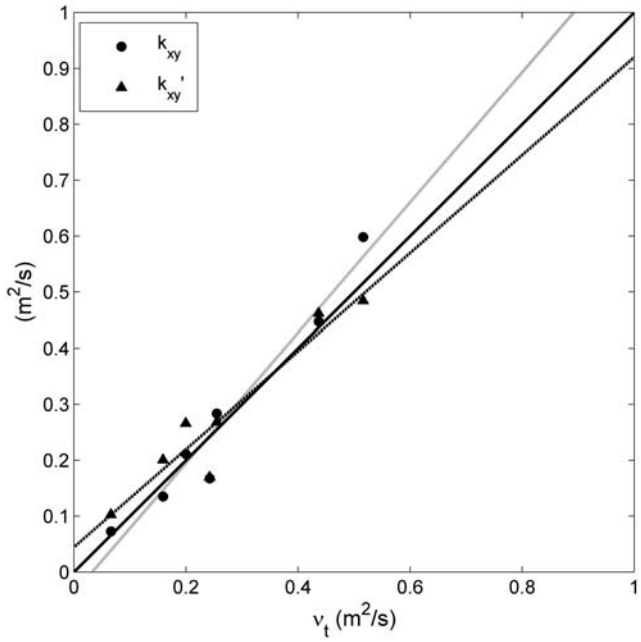

Figure 12. Turbulence intensity υ_t obtained from (20) and k_{xy}, k'_{xy} estimated with all drifters for each deployment day. Black line represents perfect correlation, the dotted line represents k_{xy} best fit (R^2 = 0.95, slope = 1.1, y intercept = −0.02), and the gray line represent k'_{xy} best fit (R^2 = 0.95, slope = 0.88, y intercept = 0.04).

shore diffusivities for the alongshore current systems (2.6–4.9 m^2/s) are larger than those observed by *Spydell et al.* [2007] (0.7–1.5 m^2/s) though they decrease to more comparable values at later times (0.1–2.5 m^2/s). On days exhibiting the same flow pattern, absolute diffusivities are smaller for days with smaller waves and shorter periods, resembling *Spydell et al.* [2007], though the exact relationship between flow pattern, wave conditions and diffusivity cannot be generalized due to the lack of data. The cross-shore diffusivity on yearday 139 exemplifies the difference bathymetric variations and flow pattern can make on the diffusivity. Wave heights and period are similar to day 1 of *Spydell et al.* [2007], but the sinuous alongshore flow over the rip channeled bathymetry restricts particle dispersion to the surf zone and the cross-shore diffusivity falls to zero, while for near-planar bathymetry for *Spydell et al.* [2007], the cross-shore diffusivity reaches a nonzero asymptote.

[46] The trends of two-particle statistics D_p and K_p relative to t and d calculated for RCEX and those obtained by *Spydell et al.* [2007] are similar, though there are differences in the shape of the individual curves. *Spydell et al.* [2007] calculated a relationship of $D^2 \sim t^{3/2}$, close to the $D^2 \sim t^{4/3}$ calculated at RCEX. For our results, D^2_{px} and D^2_{py} do not expand at similar rates initially for rip current flow fields. D^2_{px} is larger until the alongshore dispersion increases and D^2_{py} becomes equal then larger at t > 300 s. For the meandering and sinuous alongshore flow fields the relationship between D^2_{px} and D^2_{py} is more similar to *Spydell et al.* [2007], as expected due to the presence of a dominant alongshore current. The value of λ = 0.04–0.2 computed over small separations before the particles become decorrelated is smaller than the value of 0.66 found by *Spydell et al.* [2007], but both are weaker than Richardson-like behavior (λ = 4/3). The actual shape of the K_{pi} curves are not similar at all, with the curves calculated for the rip current environment growing steadily before reaching an asymptote as the particle spreading reaches a maximum and particles begin to contract rather than spread. Asymptotic values of K_p (1.5–6.5 m^2/s) are generally larger than those found by *Johnson and Pattiaratchi* [2004] (0.7–1.9 m^2/s) for rip current flow patterns and the values of K_{px} are greater than K_{py}, unlike *Johnson and Pattiaratchi* [2004]. The computed values of K_p from RCEX demonstrate none of the Richardson-like scale dependence they found.

[47] Calculations of average cluster diffusivity over different temporal intervals on days with rip current flow patterns (K_e = 1.7–3.6 m^2/s) compare well with those found by *Johnson and Pattiaratchi* [2004]. The calculations of these interval diffusivities is a somewhat arbitrary process since calculating the diffusivity this way is sensitive to the points chosen for the calculation. For comparison, the mean diffusivity calculated from the total patch spread over the entire deployment is found to be ∼0.5 m^2/s for the four deployments of *Johnson and Pattiaratchi* [2004]. This representative value is generally smaller than the values found for the rip current patterns observed during RCEX. It is expected that the quasi-permanent features of the rip current flow fields would produce more dispersion than transient rip currents described by *Johnson and Pattiaratchi* [2004]. The oscillations in K_{ex} and K_{ey} are similar for transient and morphological rip currents.

7.2. Small-Scale Turbulent Diffusivity Within the Surf Zone

[48] Waves are the primary driving force for motions within the surf zone. Wave driven motions include mean alongshore currents, rip currents and undertow, long period motions such as infragravity waves and very low frequency vortical motions forced by the wave groups and wave gradients, orbital wave motions and breaking wave-induced turbulence. These wave-induced mean and long period motions create large-scale shear that result in dispersion at the larger scale, and the breaking waves create small-scale turbulence that results in dispersion at the smaller scale. Since these motions are at well separated time and space scales, they can be assumed uncorrelated [*Trowbridge*, 1998].

[49] Two independent methods are used to estimate diffusivities owing to the small-scale (both in time and space) turbulence that give similar values. Using a two-step process to separate the length [*Okubo and Ebbesmeyer*, 1976] and time scales [*List et al.*, 1990], it is found that small-scale turbulent relative diffusivities of clusters, k_{xy}, are constant throughout a deployment day (Table 5); this indicates that the background turbulent contribution remains constant for constant wave conditions and that the method is robust. Small-scale turbulent diffusivities are also obtained by integrating the autocovariance function of the drifter velocities measured from the one-particle velocity statistics over a short time, k'_{xy}, which gave consistent results with the two-step separation process providing confidence in the methodologies. An approximate time scale of the turbulence is the microscale obtained by fitting a parabola to the autocorrelation function as $\tau \rightarrow 0$ [*Tennekes and Lumley*, 1972],

Table 7. Ratio of Relative Diffusivity to Turbulent Eddy Diffusivity[a]

Yearday	mean(K_e/k_{xy}) (m^2/s)
117	8.6
124	9.5
125	2.9
127	29.2
130	19.9
135	22.3
139	16.9

[a]Here mean(K_e/k_{xy}) is the mean ratio of relative diffusivity computed by the cluster method to the turbulent eddy diffusivity.

which gives a time scale $<T_p$, the peak wave period. A scale of the wave period can also be observed in the oscillations of the autocovariance functions (Figures 3a, 3e, 3i, and 3m) that is attributed to the repetitious impulse of turbulence at the breaking wave period.

[50] The two estimated small-scale eddy diffusivities k_{xy}, k'_{xy} are significantly correlated with each other and with calculated eddy viscosity based on the average breaking wave dissipation and turbulence production over the surf zone [*Battjes*, 1975] that is a function of input wave energy flux and surf zone width (which in turn is a function of the breaking wave height, tidal elevation and beach slope). Within the surf zone, (20) gives $\upsilon_t \sim \tan\beta^{1/3} H^{3/2}$, indicating the small-scale turbulent eddy diffusivities are a strong function of wave height and a weak function of the beach slope, $\tan\beta$. Slope dependence is expected as the result of incorporating an average energy dissipation across the surf zone to describe the eddy viscosity in (20) where mean energy dissipation density increases with increased beach slope resulting in a narrower surf zone width for the same breaking wave height.

[51] In the derivation of (20), it was assumed by *Battjes* [1975] that the near isotropic turbulence generated by the breaking waves is in the presence of a shear current (alongshore current or rip current in this case) and that the current causes a stretching of the turbulent eddies. The axes of the eddies contributing most to the resulting stress and momentum mixing are expected to be aligned with the axis of the principal strain rate of the mean flow, which results in horizontal eddies (vortices) with vertical axes. The characteristic size of the vortices will be limited by vertical extent of the turbulence as given by the local depth or in this case the wave height. Subsequently *Nadaoka et al.* [1989] found near-vertical turbulent vortices after the passage of spilling breakers in the laboratory in the absence of currents. These descending vortices in the horizontal plane with vertical axes reach down toward the bottom. The process of generating these eddies is not well understood, but the time scales less than the wave period and length scale equal to or less than the local depth are in accord with the formulation of *Battjes* [1975] and the measurements here. It is noted that the Delft 3-D circulation model applied to the nearshore gives good predictions of long period motions of edge waves and very low frequency motions using the *Battjes* [1975] formulation for eddy viscosity to describe the turbulent momentum transfer in the horizontal [*Reniers et al.*, 2006, 2007].

[52] Other mixing mechanisms not included here are associated with the vertical structure of currents. It was shown that the interaction of the vertical structures of mean alongshore and cross-shore undertow [*Svendsen and Putrevu*, 1994] and of the shear instabilities of the alongshore current and the alongshore flow [*Zhao et al.*, 2003] can result in gradients in the mean horizontal momentum, i.e., $\int \overline{\rho u(z,t)v(z,t)}\, dz$ inducing horizontal mixing. Since the measurements presented here represent horizontal surface currents the unknown contribution by the vertical structure is not assessed.

[53] The diffusivity calculated from the cluster statistics, K_e, represents diffusivity for all the physical processes combined, whereas k_{xy}, k'_{xy} represent diffusivity for breaking wave generated small-scale turbulence. K_e values are 3–30 times larger than k_{xy} (Table 7), k'_{xy} depending on the day suggesting that the shear of the larger-scale motions is responsible for most of the dispersion.

8. Conclusions

[54] Rip currents initially disperse material rapidly (κ_{xx} = 5.4–6.1 m^2/s) across the surf zone owing to large current velocities and high shear. The restriction of the rip current circulation recollects the material after this rapid expansion, slowing the diffusion to an asymptotic rate (κ_{xx} = 0.9–2.2 m^2/s) with the contraction balanced by the expansion as material begins to recirculate. The drifters are able to move between rip current cells in the alongshore so that eventually the diffusion in the alongshore will surpass the cross-shore diffusion (κ_{yy} = 2.8–3.8 m^2/s). The absolute diffusivity measurements represent the displacement of a tracer from its release point similar to dye experiments and compare well with previous dye cross-shore measurements though unlike the dye measurements, alongshore diffusivity is larger than cross shore found by *Inman et al.* [1971]. Peaks in the cross-shore diffusivity are related to the rotation time (~300 s) of the rip current.

[55] Two-particle statistics, quantifying the spread of particles relative to each other, determined initial patch spread is in the cross shore before the patch becomes circular then alongshore polarized. Cross-shore relative diffusivity (K_{px} = 1–6.5 m^2/s) was larger than alongshore relative diffusivity (K_{py} = 0.4–3.9 m^2/s) for t < 300 s. Similar to other surf zone drifter experiments [*Spydell et al.*, 2007], the circulation patterns observed behaved in a weaker than Richardson-like manner, $D^2 \sim t^{4/3}$. Calculations of the diffusivity with cluster and two particle statistics show significant correlation ($R^2 > 0.9$) suggesting that the two methods are comparable [*LaCasce*, 2008], even in a nonhomogeneous flow field. The calculations of D_{ex} and D_{ey} demonstrate the contraction and expansion that occur within a group of drifters as they move through different parts of the rip current circulation cell, spreading in the cross shore while centered in the rip channel and over the shoal and spreading in the alongshore when centered in the alongshore flow portion.

[56] The two independent methods to calculate small-scale turbulent diffusivity, k_{xy} and k'_{xy}, provide consistent estimates of the turbulent eddy diffusivity (k_{xy} = 0.1–0.6 m^2/s) with smaller values associated with smaller wave heights driving weaker currents. The estimated turbulent eddy diffusivities are strongly correlated (R^2 = 0.95) with the estimated surf zone averaged wave-breaking induced turbulent

eddy viscosity, υ_t. The calculated shear contribution to diffusion is generally an order of magnitude greater than the small-scale turbulent diffusivity, $K_e/k_{xy} = 3-30$ (Table 7). The diffusivity of the surf zone is dependent on a number of factors including the flow pattern and wave conditions that are present. In general, flow patterns with less shear and slower velocities with smaller waves exhibit smaller levels of diffusion.

[57] **Acknowledgments.** We extend our appreciation to the many folks who assisted in obtaining drifter data set: Tim Stanton, Jenna Brown, Jon Morrison, Edie Gallagher, Jim Stockel, Rob Wyland, Keith Wyckoff, Ron Cowen, Natalie Lauder, Mark Orzech, Nick Dodd, Jim Lambert, and Lance Valenzuela. This work was funded through the Office of Naval Research Coastal Geosciences Program, Delaware Sea Grant, California State Coastal Conservancy, and National Science Foundation. The field experiment, travel support, and PI and staff support (Stanton, Stockel, Wyland, Wyckoff, and Cowen) was provided by ONR N0001407WR20226 and N0001408WR20006. Supporting experimental infrastructure (directional wave and video observed) was funded in part by the California State Coastal Conservancy as part of the Coastal Ocean Circulation Monitoring Program-Northern California under contract 04–034. J.M. was supported by ONR contracts N00014-05-1-0154, N00014-05-1-0352, N0001407WR20226, and N0001408WR20006 and the National Science Foundation OCE 0728324. J.B. was supported by the Delaware Sea Grant, University of Delaware, and ONR N0001407WR20226 and N0001408WR20006. A.R. was supported by ONR N000140710556 and the University of Miami. E.T. was supported by ONR N0001407WR20226. Constructive suggestions from two anonymous reviewers are greatly appreciated.

References

Batchelor, G. K. (1950), The application of the similarity theory of turbulence to atmospheric diffusion, *Q. J. R. Meteorol. Soc.*, *76*, 133–146, doi:10.1002/qj.49707632804.

Batchelor, G. K., and A. A. Townsend (1956), Turbulent diffusion, in *Surveys in Mechanics: A Collection of Surveys of the Present Position of Research in Some Branches of Mechanics*, edited by G. K. Batchelor and R. M. Davies, pp. 352–399, Cambridge Univ. Press, Cambridge, U. K.

Battjes, J. A. (1975), Modeling of turbulence in the surf zone, paper presented at Symposium on Modeling Technology, Am. Soc. of Civ. Eng., San Francisco, Calif.

Bendat, J. S., and A. G. Piersol (2000), *Random Data, Analysis and Measurement Procedures*, 594 pp., Wiley Intersci., New York.

Boffetta, G., and I. M. Sokolov (2002a), Relative dispersion in fully developed turbulence: The Richarson's law and intermittency corrections, *Phys. Rev. Lett.*, *88*, 094501.1–094501.4.

Boffetta, G., and I. M. Sokolov (2002b), Statistics of two-particle dispersion in two-dimensional turbulence, *Phys. Fluids*, *14*, 3224–3232.

Clarke, L. B., D. Ackerman, and J. Largier (2007), Dye dispersion in the surfzone: Measurements and simple models, *Cont. Shelf Res.*, *27*, 650–669, doi:10.1016/j.csr.2006.10.010.

Davis, R. E. (1985), Drifter observations of coastal surface currents during CODE: The method and descriptive view, *J. Geophys. Res.*, *90*, 4741–4755, doi:10.1029/JC090iC03p04741.

Davis, R. E. (1987), Modeling eddy transport of passive tracers, *J. Mar. Res.*, *45*, 635–665, doi:10.1357/002224087788326803.

Drinkwater, K. F., and J. W. Loder (2001), Near-surface horizontal convergence and dispersion near the tidal-mixing front on northeastern Georges Bank, *Deep Sea Res. Part II*, *48*, 311–339, doi:10.1016/S0967-0645(00)00084-9.

Grant, S., J. H. Kim, B. H. Jones, S. A. Jenkins, and J. Wasyl (2005), Surf zone entrainment, along-shore transport, and human health implications of pollution from tidal outlets, *J. Geophys. Res.*, *110*, C10025, doi:10.1029/2004JC002401.

Inman, D. L., R. J. Tait, and C. E. Nordstrom (1971), Mixing in the surfzone, *J. Geophys. Res.*, *76*, 3493–3514, doi:10.1029/JC076i015p03493.

Johnson, D., and C. Pattiaratchi (2004), Transient rip currents and nearshore circulation on a swell-dominated beach, *J. Geophys. Res.*, *109*, C02026, doi:10.1029/2003JC001798.

Johnson, D., R. Stocker, R. Head, J. Imberger, and C. Pattiaratchi (2003), A compact, low-cost GPS drifter for use in the oceanic nearshore zone, lakes, and estuaries, *J. Atmos. Oceanic Technol.*, *20*, 1880–1884, doi:10.1175/1520-0426(2003)020<1880:ACLGDF>2.0.CO;2.

Jullien, M.-C., J. Paret, and P. Tabeling (1999), Richardson pair dispersion in two-dimensional turbulence, *Phys. Rev. Lett.*, *82*, 2872–2875, doi:10.1103/PhysRevLett.82.2872.

LaCasce, J. H. (2008), Lagrangian statistics from oceanic and atmospheric observations, *Lect. Notes Phys.*, *744*, 165–218, doi:10.1007/978-3-540-75215-8_8.

LaCasce, J. H., and A. Bower (2000), Relative dispersion in the subsurface North Atlantic, *J. Mar. Res.*, *58*, 863–894, doi:10.1357/002224000763485737.

List, E. J., G. Gartrell, and C. D. Winant (1990), Diffusion and dispersion in coastal waters, *J. Hydraul. Eng.*, *116*, 1158–1179, doi:10.1061/(ASCE)0733-9429(1990)116:10(1158).

MacMahan, J., E. B. Thornton, T. P. Stanton, and A. J. H. M. Reniers (2005), RIPEX—Rip currents on a shore-connected shoal beach, *Mar. Geol.*, *218*, 113–134, doi:10.1016/j.margeo.2005.03.019.

MacMahan, J. H., E. B. Thornton, and A. J. H. M. Reniers (2006), Rip current review, *Coastal Eng.*, *53*, 191–208, doi:10.1016/j.coastaleng.2005.10.009.

MacMahan, J., et al. (2009a), Mean Lagrangian flow behavior on an open coast rip-channeled beach: New perspectives, *Mar. Geol.*, doi:10.1016/j.margeo.2009.09.011, in press.

MacMahan, J., J. Brown, and E. B. Thornton (2009b), Low-cost handheld Global Positioning Systems for measuring surf zone currents, *J. Coastal Res.*, *25*, 744–754, doi:10.2112/08-1000.1.

Manning, J. P., and J. H. Churchill (2006), Estimates of dispersion from clustered-drifter deployments on the southern flank of Georges Bank, *Deep Sea Res. Part II*, *53*, 2501–2519, doi:10.1016/j.dsr2.2006.08.004.

Nadaoka, K., M. Hino, and Y. Koyano (1989), Structure of the turbulent flow field under breaking waves in the surf zone, *J. Fluid Mech.*, *204*, 359–387, doi:10.1017/S0022112089001783.

Obukhov, A. M. (1941a), Spectral energy distribution in a turbulent flow, *Dokl. Akad. Nauk SSSR*, *32*, 22–24.

Obukhov, A. M. (1941b), Spectral energy distribution in a turbulent flow, *Izv. Akad. Nauk SSSR Ser. Fiz.*, *5*, 453–466.

Okubo, A. (1971), Oceanic diffusion diagrams, *Deep Sea Res.*, *18*, 789–802.

Okubo, A., and C. C. Ebbesmeyer (1976), Determination of vorticity, divergence, and deformation rates from analysis of drogue observations, *Deep Sea Res.*, *23*, 349–352.

Reniers, A. J. H. M., J. Mac, J. Mahan, E. B. Thornton, and T. P. Stanton (2006), Modeling infragravity motions on a rip-channel beach, *Coastal Eng.*, *53*(2–3), 209–222, doi:10.1016/j.coastaleng.2005.10.010.

Reniers, A. J. H. M., J. H. MacMahan, E. B. Thornton, and T. P. Stanton (2007), Modeling of very low frequency motions during RIPEX, *J. Geophys. Res.*, *112*, C07013, doi:10.1029/2005JC003122.

Richardson, L. F. (1926), Atmospheric diffusion shown on a distance-neighbour graph, *Proc. R. Soc. London Ser. A*, *110*, 709–737, doi:10.1098/rspa.1926.0043.

Sanderson, B. G. (1995), Structure of an eddy measured by drifters, *J. Geophys. Res.*, *100*, 6761–6776, doi:10.1029/94JC03006.

Schmidt, W. E., B. T. Woodward, K. S. Millikan, R. T. Guza, B. Raubenheimer, and S. Elgar (2003), A GPS-tracked surf zone drifter, *J. Atmos. Oceanic Technol.*, *20*, 1069–1075, doi:10.1175/1460.1.

Schmidt, W. E., R. T. Guza, and D. N. Slinn (2005), Surf zone currents over irregular bathymetry: Drifter observations and numerical simulations, *J. Geophys. Res.*, *110*, C12015, doi:10.1029/2004JC002421.

Shepard, F. P., K. O. Emery, and E. C. La Fond (1941), Rip currents: A process of geological importance, *Eos Trans. AGU*, *31*(4), 555–565.

Smith, P. C. (1989), Circulation and dispersion on Browns Bank, *Can. J. Fish. Aquat. Sci.*, *46*, 539–559, doi:10.1139/f89-073.

Spydell, M., F. Feddersen, R. Guza, and W. Schmidt (2007), Observing surfzone dispersion with drifters, *J. Phys. Oceanogr.*, *37*(12), 2920–2939, doi:10.1175/2007JPO3580.1.

Svendsen, I. A., and U. Putrevu (1994), Nearshore mixing and dispersion, *Proc. R. Soc. London Ser. A*, *445*, 561–576, doi:10.1098/rspa.1994.0078.

Taylor, G. I. (1922), Diffusion by continuous movements, *Proc. London Math. Soc.*, *s2-20*, 196–212, doi:10.1112/plms/s2-20.1.196.

Tennekes, H., and J. L. Lumley (1972), *A First Course in Turbulence*, 300 pp., MIT Press, Cambridge, Mass.

Trowbridge, J. H. (1998), On a technique for measurement of turbulent shear stress in the presence of surface waves, *J. Atmos. Oceanic Technol.*, *15*, 290–298, doi:10.1175/1520-0426(1998)015<0290:OATFMO>2.0.CO;2.

Tseng, R. S. (2002), On the dispersion and diffusion near estuaries and around islands, *Estuarine Coastal Shelf Sci.*, *54*, 89–100, doi:10.1006/ecss.2001.0830.

Veneziani, M., A. Griffa, A. M. Reynolds, and A. J. Mariano (2004), Oceanic turbulence and stochastic models from subsurface Lagrangian data for the northwest Atlantic Ocean, *J. Phys. Oceanogr.*, *34*, 1884–1906, doi:10.1175/1520-0485(2004)034<1884:OTASMF>2.0.CO;2.

Veneziani, M., A. Griffa, Z. D. Garraffo, and E. P. Chassignet (2005a), Lagrangian spin parameter and coherent structures from trajectories released in a high-resolution ocean model, *J. Mar. Res.*, *63*, 753–788, doi:10.1357/0022240054663187.

Veneziani, M., A. Griffa, A. M. Reynolds, Z. D. Garraffo, and E. P. Chassignet (2005b), Parameterizations of Lagrangian spin statistics and particle dispersion in the presence of coherent vortices, *J. Mar. Res.*, *63*, 1057–1083, doi:10.1357/002224005775247571.

Zhao, Q., I. A. Svendsen, and K. Hass (2003), Three-dimensional effects in shear waves, *J. Geophys. Res.*, *108*(C8), 3270, doi:10.1029/2002JC001306.

J. Brown, Civil and Environmental Engineering, University of Delaware, 301 DuPont Hall, Newark, DE 19716, USA.

J. MacMahan and E. Thornton, Oceanography Department, Naval Postgraduate School, Monterey, CA 93943, USA. (jhmacmah@nps.edu)

A. Reniers, Applied Marine Physics, Rosenstiel School of Marine and Atmospheric Science, University of Miami, 4600 Rickenbacker Causeway, Miami, FL 33149, USA.